VYSOKÉ UČENÍ TECHNICKÉ V BRNĚ
BRNO UNIVERSITY OF TECHNOLOGY

FAKULTA ELEKTROTECHNIKY A KOMUNIKAČNÍCH TECHNOLOGIÍ
ÚSTAV BIOMEDICÍNSKÉHO INŽENÝRSTVÍ

FACULTY OF ELECTRICAL ENGINEERING AND COMMUNICATION
DEPARTMENT OF BIOMEDICAL ENGINEERING

SYNTHESIS OF SIO2/AU CORE/SHELL NANOPARTICLES FOR ENHANCEMENT OF OCT SIGNAL

SYNTÉZA SIO$_2$/AU CORE/SHELL NANOČÁSTIC PRO ZESÍLENÍ OCT SIGNÁLU
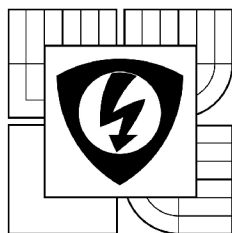
DIPLOMOVÁ PRÁCE
MASTER´S THESIS

AUTOR PRÁCE   Bc. MARTINA KANTOROVÁ
AUTHOR

VEDOUCÍ PRÁCE   Ing. JANA DRBOHLAVOVÁ, Ph.D.
SUPERVISOR

BRNO 2015

BRNO UNIVERSITY
OF TECHNOLOGY

Faculty of Electrical Engineering and
Communication

Department of Biomedical Engineering

Diploma thesis

Master's study field
Biomedical Engineering and Bioinformatics

Student: Bc. Martina Kantorová   *ID:* 127459
Year of study: 2   *Academic year:* 2014/15

TITLE OF THESIS:

Synthesis of SiO2/Au core/shell nanoparticles for enhancement of OCT signal

INSTRUCTION:

1) Study the application of nanoparticles in optical coherent tomography (OCT) for signal enhancement. Provide a literature survey about synthesis method of SiO2/Au core/shell nanoparticles for above mentioned application. Find the essential parameters which are required to achieve the maximal monodispersity of silica nanoparticles as well as their uniform surface coverage by gold. 2) Study the analytical methods suitable for characterization of physical and chemical properties of SiO2/Au core/shell nanoparticles, including size, composition and mainly optical properties. 3) Make a proposal of your own protocol of nanoparticles laboratory synthesis. 4) Prepare and characterize the nanoparticles. 5) Discuss your results with regard to application in enhancement of OCT signal. Compare the results with relevant scientific publications. Make a conclusion and suggest the optimization of preparation if necessary.

REFERENCE:

[1] BRINSON, B. E., et al. "Nanoshells Made Easy: Improving Au Layer Growth on Nanoparticle Surfaces." Langmuir, 2008, roč. 24, s. 14166-14171. ISSN: 0743-7463
[2] NIKABADI, H. R., et al. "Gradual growth of gold nanoseeds on silica for SiO2@gold homogeneous nano core/shell applications by the chemical reduction method." Physica Scripta, 2013, roč. 87, č. 2, s. 341-345. ISSN: 0928-0707

Assigment deadline: 9. 2. 2015   *Submission deadline:* 31.7.2015

Head of thesis: Ing. Jana Drbohlavová, Ph.D.
Consultant: Assoc. Prof. Roberto Llorente

prof. Ing. Ivo Provazník, Ph.D.
WARNING: *Subject Council chairman*

Prohlášení

Prohlašuji, že diplomová práce na téma syntéza SiO_2/Au jadro/obal nanočastíc pro zesílení OCT signálu jsem vypracovala samostatně pod vedením vedoucího semestrálního projektu a s použitím odborné literatury a dalších informačních zdrojů, které jsou všechny citovány v práci a uvedeny v seznamu literatury na konci práce. Jako autor uvedené závěrečné práce dále prohlašuji, že v souvislosti s vytvořením této práce jsem neporušila autorská práva třetích osob, zejména jsem nezasáhla nedovoleným způsobem do cizích autorských práv osobnostních a jsem si plně vědoma následků porušení ustanovení § 11 a následujících autorského zákona č. 121/2000 Sb., včetně možných trestněprávních důsledků vyplývajících z ustanovení § 152 trestního zákona č. 140/1961 Sb.

V Brně dne 31.07. 2015

....

podpis autora

Poďakovanie

Chcela by som poďakovať vedúcej mojej diplomovej práce Ing. Jane Drbohlavovej, Ph.D. za jej ochotu, podporu, vecné rady a hlavne trpezlivosť. Ďalej by som chcela poďakovať svojej rodine a priateľovi, ktorí pri mne stáli a podporovali ma.

V Brne dňa 31.07.2015

....

podpis autora

Abstrakt

Cieľom diplomovej práce je syntéza SiO2/Au jadro/obal nanočastíc. Tieto nanočastice by mali vylepšovať signál optickej koherentnej tomografie (OCT). V práci je popísaná metóda syntézy nanočastíc. Vlastnosti vyrobených nanočastice boli analyzované skenujúcim elektrónovým mikroskopom (SEM), Ultrafialovým viditeľným spektrometrom (UV-Vis), Blízkym infračerveným spektroskopom (NIRS), Fourierovým transformačným infračerveným spektroskopom (FT-IR) a metódou dynamického rozptylu svetla (DLS). V ďalšom bode práce boli nanočastice testované pre vylepšenie signálu optickej koherentnej tomografie. Pre toto testovanie boli použité taktiež komerčné nanočastice s rovnakou štruktúrou a veľkosťou.

Kľúčové slová

Syntéza SiO2/Au jadro/obal nanočastíc, SEM, FT-IR, UV-Vis, NIRS, DLS, zosílenie OCT signálu

Abstract

The aim of this master thesis is synthesis of SiO2/Au core/shell nanoparticles. These nanoparticles should improve the signal of optical coherence tomography (OCT). The procedure of nanoparticle synthesis is described in the work. Synthetized nanoparticles were analyzed by scanning electron microscopy (SEM), Ultraviolet-Visible spectroscopy (UV-Vis), Near-infrared spectroscopy (NIRS), Fourier transform-infrared spectroscopy (FT-IR) and Dynamic light scattering (DLS). Then, the synthetized nanoparticles were tested for enhancement of OCT signal. For this testing were also used commercial nanoparticles with the same structure and similar size.

Keywords

Synthesis of SiO2/AU core/shell nanoparticles, SEM, FT-IR, UV-Vis, NIRS, DLS, enhancement of OCT signal

Content

List of figures

Introduction

Nowadays, the nanoparticles are intensely explored because of the wide variety of their potential applications in optical, electronic and medical fields. In the last mentioned, they provide great technological advantages such as high stability, reduced toxicity, high surface-to-volume ratio and also tunable size which predict their physical and chemical properties suitable for targeted delivery and controlled release of molecules [1,2].

Nanoparticles as contrast agents are rapidly becoming potentially tools for improving medical diagnosis for *in vivo* imaging technologies, namely for detection or visualization the cells, tissues or organs. In comparing with conventional contrast agents, they offer improved abilities, such a longer circulations times, enhancement of targeting delivery, and multi-binding capacities [3]. They used to be made from biodegradable and biocompatible materials such gold and magnetic nanoparticles based on iron oxides, often combined with various polymers or ceramics (SiO_2). The nanoparticles are functionalized by macromolecules such as peptides, ligands, nucleotides for drug targeting and delivering to a concrete location [4,5]. The size and concentration of nanoparticles are crucial parameters for their biodistribution and circulation in the human body, cellular uptakes and ability to permeate through tissue[6].

A special focus is placed on nanoparticles for specific application for magnetic resonance imaging (MRI), positron emission tomography (PET), computed tomography (CT), ultrasound (US) or optical coherence tomography (OCT) [3,7]. This work is focused on synthesis of silica/gold core/shell nanoparticles for enhancement of OCT signal. These nanoparticles have silica core with the size around 290 nm coated by thin layer of the gold nanoshells.

This work is made up of 7 chapters. The first chapter deals with properties of silica and gold nanoparticles. It discusses optical properties of gold nanoparticles from what arises their special use in imaging modalities for enhancement signal. The chapter 2 contains synthesis approaches of nanoparticles, mainly Stöber process and method of Duff which were used for preparing of SiO_2 and Au nanoparticles. The chapter 3 presents the optical coherence tomography as an imaging modality, principle of its work and also the possibility of using SiO_2/Au core/shell nanoparticles as contrast agents in OCT. The principles of characterization methods of nanoparticles are described in chapter 4. The chapter 5 is aimed at procedure of SiO_2/Au nanoparticle synthesis. The chapter 6 offers the results of measurements; it discusses the properties of synthetized silica/gold nanoparticles as size, shape, optical properties, *etc*. It includes also the results from testing of these nanoparticles for enhancement of OCT signal. Last chapter, chapter 7, summarizes the achieved objectives of this work.

1 Nanoparticles in biomedical imaging

1.1 SiO$_2$ nanoparticles

SiO$_2$ nanoparticles play important role in biomedical applications. They act as contrast agent protectors. It is due to their structure, large specific surface and special properties. They include long-term stability (chemical and thermal), low toxicity, excellent biocompatibility, controllable particle size (generally from 5nm to 1 μm), flexible morphology and the ability of their functionalization with plenty of molecules or polymers [8-10]. The other advantage is their easy preparation.

SiO$_2$ nanoparticles have also excellent physical, chemical and optical properties. The optical absorption and emission bands, concentration of silanol groups on the silica surface are currently some of the most important parameters due to using of silica nanoparticles in the various research methods [11].

Silica nanoparticles are also attractive as carriers for drug delivery. However bare silica nanoparticles cannot act as targeted drug delivery carriers, they cannot evaluate the effect of drug release in diagnosis and treatment of disease. Hence, silica nanoparticles with core/shell structure are used, as a combination of silica and functional materials, which solves the above mentioned limitations. In this form they can be used as multifunctional platforms to realize the targeted controlled drug delivery or imaging [10,12].

SiO$_2$ nanoparticles were studied in combination with the nanoscale dimension of metal and semiconductor material according to their different properties and sizes. *Figure 1* shows a SEM image of SiO$_2$/Au core/shell nanoparticle [13] and its structure [14]. Silica/metal core/shell nanostructures have diverse applications which make them attractive especially for catalytic, optical and chemical sensors, biosensors, markers for bioimaging, photothermal therapy or colorimetric diagnostics or controlled release, etc. [15].
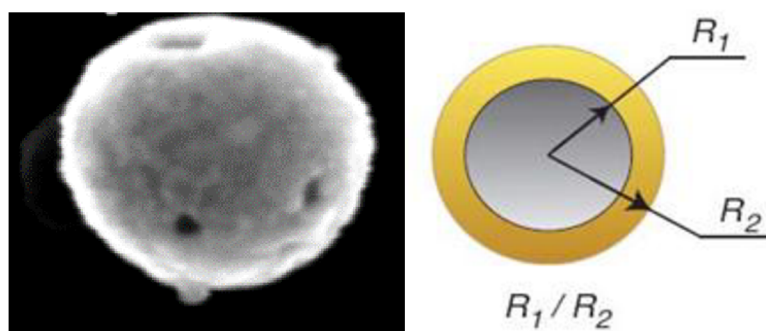
Figure 1:SEM image of SiO2/Au nanoparticles (right)[13]; structure of silica/gold core/shell nanoparticles and multilayered nanoparticles (left) [14]

1.2 Gold nanoparticles

Metal nanoparticles, depending on their concrete material, have lot of useful properties and serve as attractive tool in the field of medicine. They have properties equivalent to their bulk material, but their smaller size in comparing with a bulk compound increase their active surface area, which is convenient for further immobilization of various functional compounds [16-18].

Gold nanoparticles belong to the most stable metal nanoparticles. Their tunable optical and biocompatible properties can be manipulated for required applications. This diversity of using depends mainly on their size, shape and structure. Nowadays there are many approaches to produce the gold nanoparticles. In general, these nanoparticles can be prepared via quick and easy procedures which will be described in the *chapter 2.2* below. They combine knowledge of biology, chemistry and physics and on the basis of this knowledge it is possible to control the size and whole structure of the nanoparticles. By modification in the conditions of gold nanoparticles synthesis it is possible to achieve various shapes of nanoparticles, such as wires, plates, rods, prisms, cubes, polyhedral and branched particles [19]. These various shapes are illustrated in *Figure 2* [20].
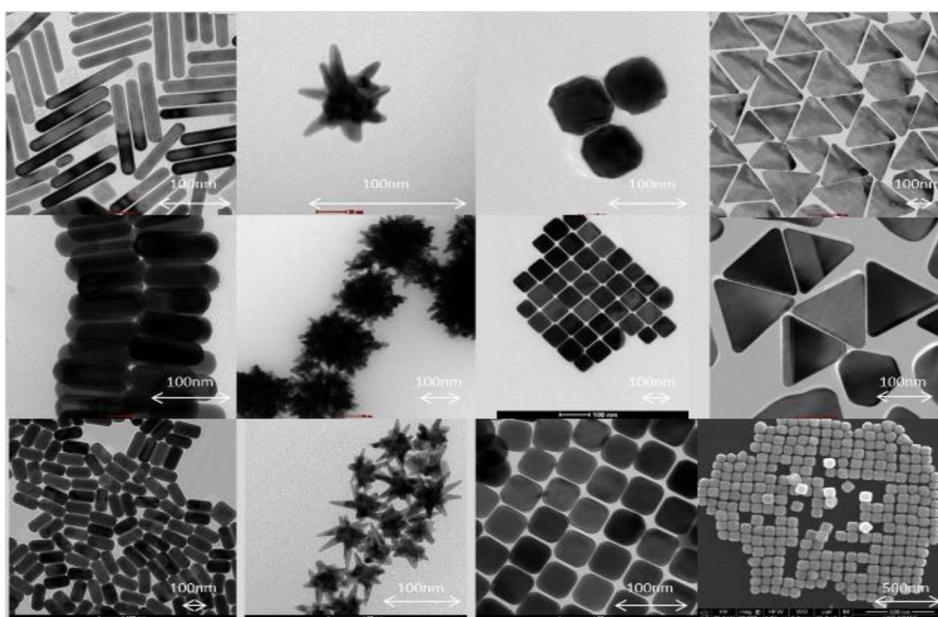
Figure 2: SEM/TEM images of various shapes of gold nanoparticles [20]

Recently, there is incredible growth in research of gold nanoparticles in the fields of bioimaging [21], bioengineering and molecular biology. Gold nanoparticles are investigated as photothermal agents, immunoassays, contrast agents or drug and antigens carriers. They are suitable as contrast agents due to their small size, ability to bind targeting agents, long retention time and mainly they offer special optical properties. Gold nanoparticles have extremely strong optical absorption or scattering of the light in the visible and NIR spectrum

of wavelength. Therefore, they are promising tool for enhancement of signal in reflectance-based diagnostic methods. That is due to the localized surface plasmon resonance (LSPR) of nanoparticles [2,22].

1.2.1 Plasmon resonance of gold nanoparticles

After an irradiance of metal particle by light, the oscillating electric field of the light causes the coherent oscillation of the conduction band electrons in the metal. If a cloud of electron moves relatively to the nucleus, a restoring force between cloud and nucleus will tend to bring the system back to equilibrium. This results in the oscillation of the electron cloud relative to the nucleus. Collective oscillation of the electrons around the surface of particles induces a charge separation which forms a dipole oscillation in the direction of the light field. This is illustrated in *Figure 3 [23]*. Higher process of plasmon oscillation, quadrupole oscillation, can happen if half of the electrons moves parallel to the field and another half of electrons moves antiparallel [23,24].
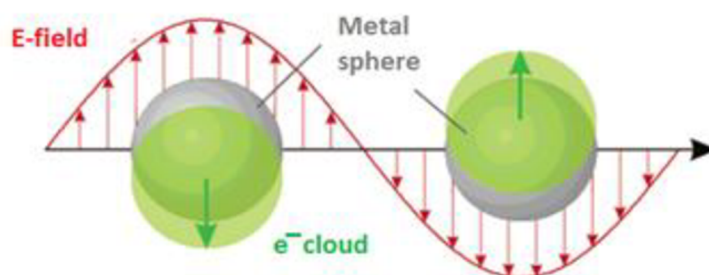
Figure 3: Schematic illustration of plasmon oscillation in metal nanoparticles [23]

The amplitude of the oscillation achieves maximum frequency at a concrete frequency which is called surface plasmon resonance (SPR). The SPR absorbs strongly the incident light hence it can be analyzed by UV-Vis spectrometer. Plasmonic (mainly gold and silver) nanoparticles, in comparing with other metal nanoparticles, have greatly stronger SPR band in visible light. Gold nanoparticles have the SPR wavelength around 520 nm, i.e. in the visible region. However the position of the SPR peak changes depending on few parameters such as particle size and shape, their structure and surface, electron density, and dielectric constant of the surrounding medium which is theoretically described by Mie theory [22-25].

An effect of SPR of small (~30 nm) gold nanoparticle causes the absorption of light in the blue-green area (~450 nm) of the spectrum and red light (~700 nm) is reflected, whereby it is obtained a rich red color. With the increasing size of nanoparticles, the wavelength of SPR shifts to longer wavelengths. Blue light it then reflected, while red light is absorbed, yielding solution of a blue/purple color. It is illustrated in *Figure 4* [26]. As particle size

increases toward the limit, wavelength of SPR move to IR spectrum and majority of the visible wavelengths are reflected, yielding in colorless solutions with nanoparticles [26].

Figure 4: Solutions of various sized monodispersed gold nanoparticles. Size of nanoparticles in solutions is increasing from the left (red color) to the right (purple color) [26]

1.2.2 Surface plasmon absorption and scattering

Absorption of the light and its scattering by these nanoparticles also with the local electric field around them, are strongly improved during the exciting of the LSPR of nanoparticles [22]. The electromagnetic wave loses energy by absorption of the light and its scattering, after the passing through a material. Process of the absorption occurs when the energy of photon is dispersed because of inelastic processes. Scattering of the light happens when this energy causes oscillations of electrons and the photons are emitted as scattered light at the same frequency as the incident light (Rayleigh scattering) or at a shifted frequency (Raman scattering). Amount of the frequency shifts equals to the difference of energy which was created by the motion of molecules in the material (vibrations, bond rotations or stretching). Both, absorption and scattering are strongly enhanced because of SPR oscillation, and largely dependent on the size of gold nanoparticles. Follow calculations are counted in the basis on Mie theory [25,27].
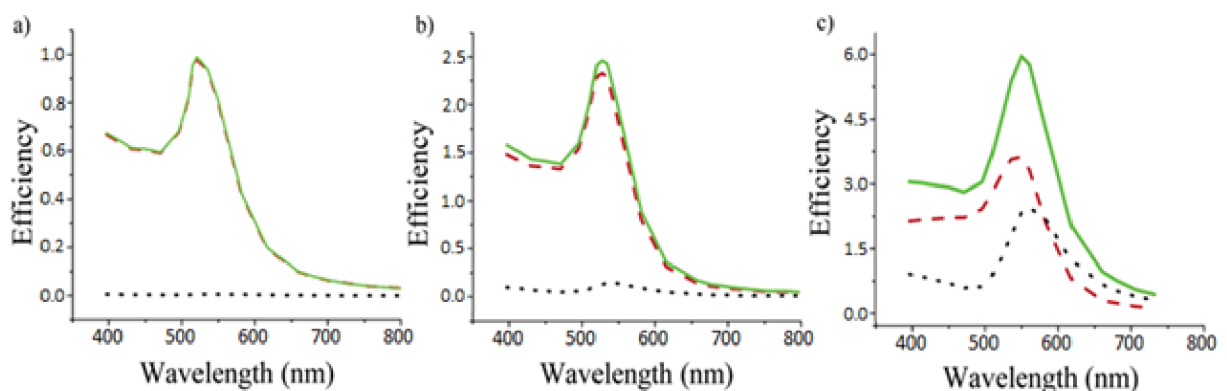
Figure 5: Calculated spectra of the efficiency of absorption (red dashed), scattering (black dotted), and extinction (green solid) for gold nanoparticles with different diameter sizes (a) 20 nm, (b) 40 nm, (c) 80 nm [24]

For the gold nanoparticles with size 20 nm, almost whole extinction of the light is caused by absorption. The scattering starts to show up with increasing the size of nanoparticles (40 nm). 80 nm diameter of gold nanoparticles absorb and scatter the light in a similar level. In the larger nanoparticles, the ratio of scattering to absorption increases dramatically. This dependence of the size for the absorption/scattering is shown in *Figure* 5 [24,27].

1.2.3 Multilayer nanoparticles

The similar procedure of synthesis as for silica/gold core/shell nanoparticles (Stöber, Duff) was employed also for the multilayer gold/silica/gold nanoparticles. Optical properties of these nanoparticles differ from those of core/shell structure mainly because of a spectral modulation of the gold core, which offers greater spectral tunability. The plasmon resonance of nanoparticles is here related to the interaction of plasmons on interfaces between gold and dielectrics (gold core-silica shell, silica shell-gold shell) [14].
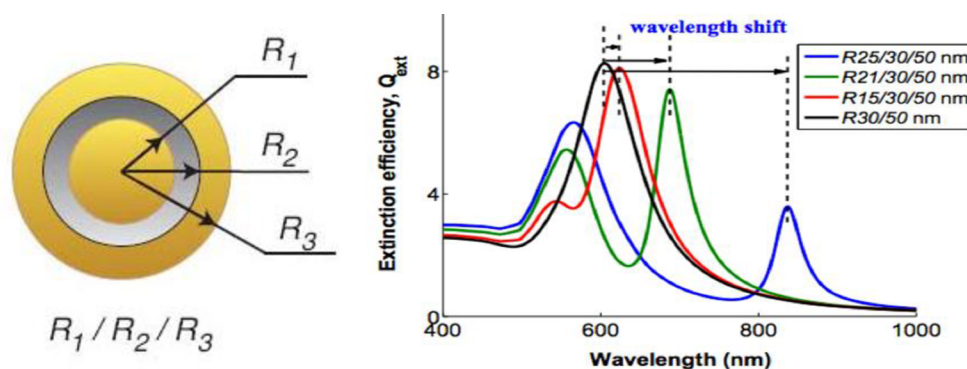
Figure 6: Multilayer structure of Au/SiO₂Au nanoparticles (left); extinction spectrum of core/shell nanoparticles and multilayer nanoparticles with different size of core and shells (right) [14]

With a 10 nm size of the gold inner gold, the scattering of nanoparticle increases with increasing of the silica layer or gold outer layer (or both). The fabricated nanoparticles with the silica layer thinner than 10 nm, exhibit more absorption than scattering. With the gold core larger than 20 nm, nanoparticles become more scattering at outer shell thickness. Larger scattering is generated also with the thicker outer gold shell. The thickness of silica layer plays here important role. With increasing size of gold nanocores (with a fixed geometry of nanoparticle) will decrease the thickness of silica layer and the plasmon interaction will increase what causes peak red-shift in the spectrum. The red-shift in the spectrum of multilayer nanoparticle can be achieved also with thicker silica layer and gold shell. Extinction spectra of the nanoparticles can be tuned by the changing of core size and shell thickness scaled by particle size. That allows the tuning of nanoshell plasmon resonances into the near-infrared (NIR) region where main biological absorption is minimal. All these spectral properties were analyzed using Mie theory.

The multiple extinction peaks of multilayer nanoparticles together with their deep spectral valleys can improve the sensitivity and specificity of bioimaging modalities. They offer more backscattering at wavelengths, in which SiO_2/Au nanoparticles mainly forwardscatter [14].

2 Nanoparticle synthesis

Nowadays, there are many different routes to fabricate nanoparticles. They can be classified in several ways, for example as chemical or physical approaches of synthesis. Nevertheless, in general, the methods to fabricate nanoparticles are divided into two fundamental approaches. These different approaches of nanoparticle synthesis are shown in *Figure 7* [28]. There is possibility to create materials with exactly required properties. The "top-down" approaches restructure a bulk material (larger precursors) to create nanoscale structures. Typical examples of this process are lithographic methods or etching methods. Top-down methods are not suitable for reduction of size to nanoscale or subatomic.

However there are "bottom-up" approaches, which are better suited to produce uniform particles with smaller scale and more complex structure. These methods create nanostructures from basic building blocks, such as atoms or molecules. In addition, they are faster, more precise and energy efficient. Inert gas condensation, sol-gel fabrication, colloidal methods, pyrolysis or structured media are common examples of bottom-up methods [29-31].
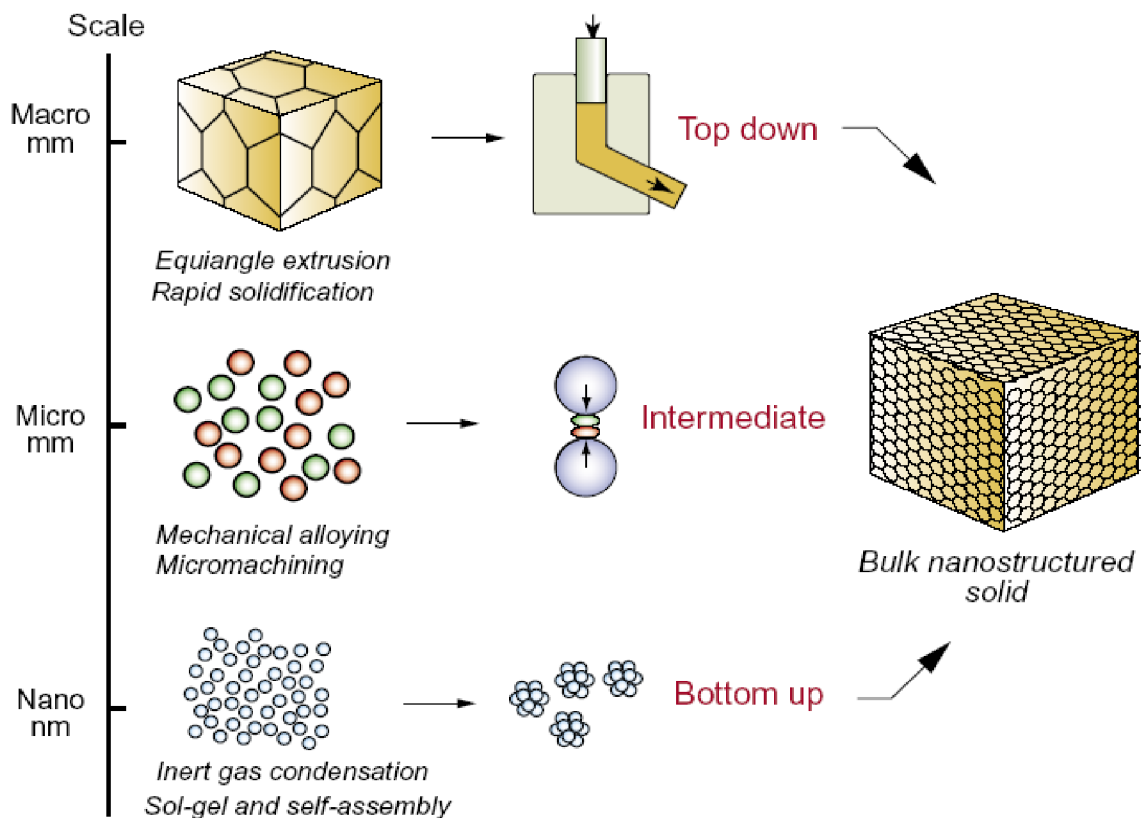
Figure 7: The top-down (physical), intermediate and bottom-up approaches (chemical) to fabricate the bulk nanostructured solids [28]

2.1 Synthesis of SiO$_2$ nanoparticles

The applications and quality of SiO$_2$ nanoparticles are strongly related to their size, shape and dispersity [32]. Hence, it is necessary to choose the synthesis method allowing production of nanoparticles with tunable size. The size can be changed by influence of various synthesis parameters(for example temperature, concentration of chemicals, silica precursors, *etc.*) [33].

The polydispersity of particles present problem in understanding and mainly in controlling fundamental properties which are necessary for example in drug delivery and release in biological systems [4]. The distribution of nanoparticles in the human body is influenced mainly by size of the nanoparticles and their surface characteristics [33].

The SiO$_2$ nanoparticles can be synthesized by different approaches. In this work, it was used sol-gel process for the preparation of nanoparticles, as it has several advantages such as control the particle size, morphology and size distribution by the monitoring of parameters in synthesis. They particularly depend on the temperature of reaction, water content or pH of the solution in reaction [29,34].

2.1.1 Sol-gel processing

Sol-gel process provides several advantages in preparation of nanoparticles such as very good control of the reaction kinetics, easy formational modification or modifiable microstructure. In this process, all formation can be split into two distinct stages, nucleation and growth. After the initial nucleation, at the stage of growth, different clusters and nanoparticles are created and serve as building blocks. Addition of monomers and their controlled aggregation to dimmer, trimmer and bigger particles, describes the mechanism of silica growth. The growth and the aggregation occur together and there not has to be noticeable difference in these two steps [35,36].

Sol-gel process leads to the development of spherical or gel network by formation of colloidal suspension, basically a dispersion of colloidal particles (sol) to liquid phase (gel). The particles react together forming 3D polymeric chain converting to this gel, which is interconnected rigid network with submicron pores and polymeric chains.

In recent years, there are used various modifications of the sol-gel process like the use of different surfactants/polymers as a template, variety of reaction conditions, techniques of drying or different precursors. The most common precursors are tetraethoxysilane (TEOS) or tetramethoxysilane (TMOS) [29].

In generally, this process involves hydrolysis and condensation reaction of metal alkoxides (TEOS, TMOS) or inorganic salts in the presence of base (NH$_3$) or acid as catalyst. There are formatted silanol groups in the hydrolysis process of TEOS molecules. All structure

is build up from siloxane bridges (Si-O-Si), which are created between silanol groups or between ethoxy groups and silanol groups [35].

One of the sol-gel methods used for synthesis of spherical and monodisperse silica nanoparticles is so called **Stöber synthesis**. Stöber *et al.* discovered this method in 1968. This method is based on hydrolysis reaction of TEOS in a mixture of water in low molecular weight alcohol in the presence of ammonia as catalyst.

This method has been explored extensively and different sizes of nanoparticles have been synthesized with the ranging from tens nanometers to a several micrometers [34]. The nanoparticles size depends on the type of alcohol, it increases with the increasing chain length of the alcohol (nanoparticles synthesized in methanol are the smallest). Also the process needs a large amount of alcohol to form a homogenous phase for the formation of monodisperse form [37]. The size of the nanoparticles is controlled by varying the concentration of TEOS and ammonia [38].

The preparation of small particles by this method is limited. There can be very high polydispersity (up to 20%) in produced nanoparticles with the size around 15–20 nm. High monodispersity, up to 3 % in deviation from the average size, has been achieved for the particles larger than 200–250 nm. It means, the monodispersity of nanoparticles is improved proportionally with the size of particles. It means, larger nanoparticles have better (higher) monodispersity.

Nevertheless Stöber method was improved by time and now seems to be the easiest and the most effective and dominant way to produce monodisperse spherical particles by modifying the reaction compositions [38].

2.2 Synthesis of Au nanoparticles

Gold nanoparticles can be prepared using various routes. More common techniques use "bottom up" methods such as chemical reduction, thermal reduction, sonochemical or electrochemical techniques, photochemical using UV irradiation, *etc.* [39].

Colloidal methods are easy way of synthesis of metal nanoparticles. These methods are included in wet chemistry processes. Ion solutions are mixed to produce non-soluble precipitates during which time temperature and pressure are controlled. Control of the nucleation and growth, nanoparticles with different sizes and morphologies can be fabricated [40]. To produce the metal nanoparticles, metal salts are reduced in solution by reducing agents (citrate, borohydride or hydrazine). Nanoparticles are further stabilized by stabilizing agents to avoid an aggregation of the nanoparticles or to improve their chemical stability.

The size, shape, and dispersity of formed nanoparticles can be affected by the variation in concentrations of the reducing agents. Size and dispersity of produced nanoparticles can be influenced also through the change of metal salt concentration [41].

2.2.1 Colloidal methods

The reduction of gold precursors in solution is one of the most common methods for the controlled morphogenesis of gold nanoparticles. It can be classified into:

- reduction of $HAuCl_4$ in the presence of water by a diversity of reducing agents:
  - sodium citrate (Turkevich et al. 1995),
  - tetrakis (hydroxymethyl) phosphonium chloride (Duff 1993),
  - sodium borohydride
- radiation-induced reduction of Au(III) ions (Gachard 1998)
- sonochemical reduction process of Au(III) ions (Mizukoshi 2000)

Turkevich method is the simplest and the most popular method of preparing monodispersed gold nanoparticles dispersed in water. This method involves the reduction of chloroauric acid ($HAuCl_4$) in a boiling sodium citrate solution (Turkevich 1951, Frens 1973). The size of nanoparticle can be tuned over a wide range of diameters by the concentration ratio between the gold salt and the sodium citrate. However polydispersity of nanoparticles increases with the size of nanoparticles [42].

In the recent years, there are new routes of synthesis, for example the citrate reduction synthesis of nanoparticles, which notably supplies a better formation of gold nanoparticles. For example by adjusting the pH of citrate solution above 6.2, it is obtained approximately monodispersity of formed nanoparticles. Hence, the citrate ions play important role here as pH mediators, which determine the final size and distribution of metal nanoparticles [43].

Many researchers employ **Duff method** for preparation of gold nanoparticles (gold colloids).This method was published by Duff in 1993. It describes the synthesis of gold nanoparticles with narrow size distribution (only few nanometers), what is a key step in the preparation of metallic nanoparticles [44].

In the process, small colloidal gold is formed from reduction of gold salt (chloroauric acid ($HAuCl_4$)) by reducing agents in the presence of water. Tetrakis (hydroxymethyl) phosphonium chloride (THPC), as a reducing agent, it serves as a primary nucleating agent, which produces a high concentration of ultrafine particles of gold (1–2 nm), without the requirement for large organic stabilizing molecules [45,46].

The particle size increases with the higher concentration of Au(III) ions in the reacting suspension, as well as with aging of the $HAuCl_4$ reagent solution [46]. Disadvantage of this method is long aging time (2–3 weeks) required to reach the red-brown color, which is characteristic for formation of gold particles [44].

3   Optical coherence tomography

Optical coherence tomography (OCT) is a new type of noninvasive optical imaging modality employing infrared light. It generates 1D depth, 2D cross-sectional and 3D volumetric images with ultrahigh-resolution. It provides structural information of sample by measuring magnitude, phase, frequency shift and polarization of backscattered or backreflected light from different layers of material in the sample. Imaging can be provided *in situ* and in real time.

OCT was demonstrated for the first time by Huang *et al.* in 1991, *in vitro* on the retina and coronary arteries [47,48]. OCT is a powerful imaging technology for medical diagnosis. It has been used for cancer imaging of the prostate, oral mucosal, gastrointestinal system [49] and also can operate for optical biopsy. One of the main applications of OCT is ophthalmology, because the penetration depth of OCT is limited only to a few millimeters in the majority of tissues. However, in the eye's fundus, the light can penetrate to the deepest layers. OCT scan of the eye is shown in *Figure 8* [50]. Another attractive field of OCT applications is endoscopy [48].
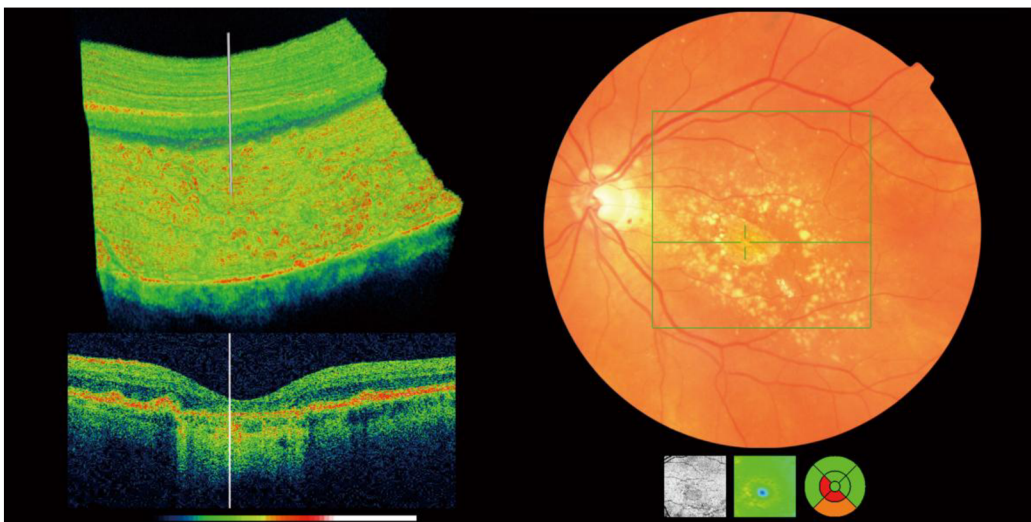
Figure 8: Cross-sectional OCT scan of a macula (left) and retinal photo (right) [50]

OCT is very similar to ultrasound imaging however it uses infrared-light instead of ultrasound waves. An advantage of OCT in comparing with ultrasonography is its resolution (10–15 μm of tissue axial resolution). Despite of limited penetration depth of OCT, it has much higher specificity and sensitivity for many characterizations, detections and visualizations of tissues.

There are two OCT systems: the first-generation system or time domain OCT and the new-generation system or Fourier domain OCT [48], which are described in details below.

3.1 Time domain OCT

A time domain OCT (TD-OCT) is a tradition optical coherence tomography. This technique uses a broadband light source. A generated near-infrared light beam is split and simultaneously directed toward an imaged tissue, where the light penetrates and reflects from the tissue, and toward an internal reference mirror. TD-OCT compares a light beam from a reference mirror to a reflected beam of light. Time delay between these beams is measured. The reference mirror moves to different distances from the source that allows an acquisition of the sample at different depths, pixel by pixel. Information about depth of the sample are obtained after a longitudinal translation in time of the reference arm [51-53]. The principle of this work is illustrated in *Figure 9.*

Scanning speed of depth can be limited by the speed of the reference mirror move. Axial resolution is under the control of OCT interference patterns and lateral resolution is limited by the numerical aperture of the optical lens of OCT [51].

The main disadvantage of TD-OCT is a mechanical process of the scanning which limits a number of captured data and also a quality of the acquired image. Images are acquired at a rate of 400 axial scans (A-scans) per second and produce one B-scan every 1.6 seconds. There are different implementations of TD-OCT depending on priority of scanning direction (transversal or depth) [54].
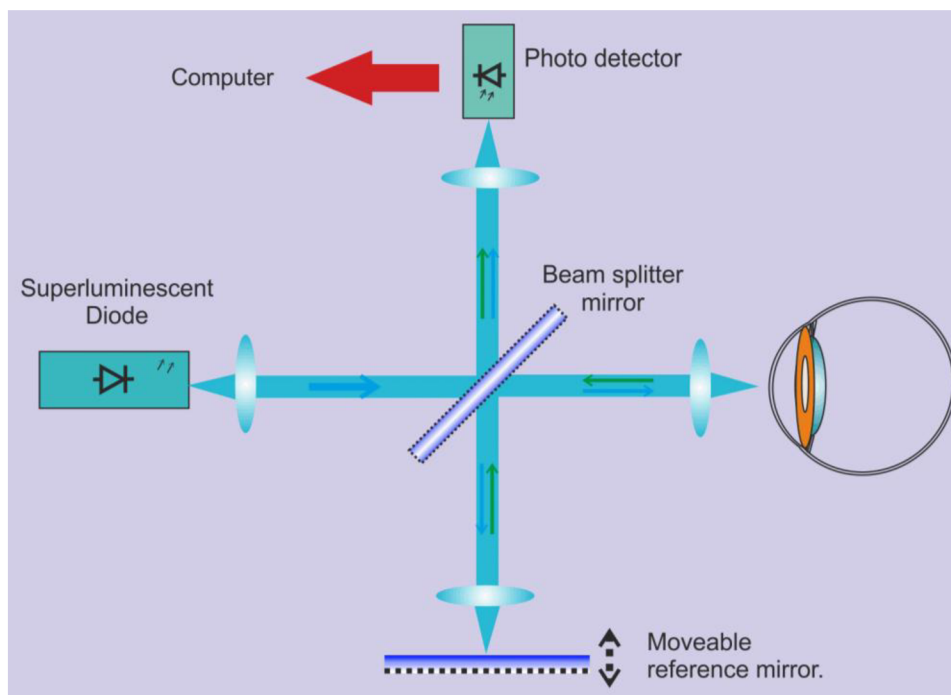
Figure 9: Time domain OCT working principle [55]

3.2 Spectral domain OCT

The recently introduced spectral domain (Fourier domain) OCT uses a different acquisition technique for obtaining 3D images of the sample, significantly faster and non-mechanical. It uses a spectrometer which measures the difference of wavelength between the backreflected light from the sample and from the fixed reference mirror. The light from the broadband source directs into the sample and illuminates it perpendicularly. The backscattered light travels to the spectrometer where the phase delay for each wavelength is detected. In this type of OCT, information about depth is acquired using a Fourier transformation. In SD-OCT, the reflected light is analyzed using a spectrometer instead a moving of reference arm [54].
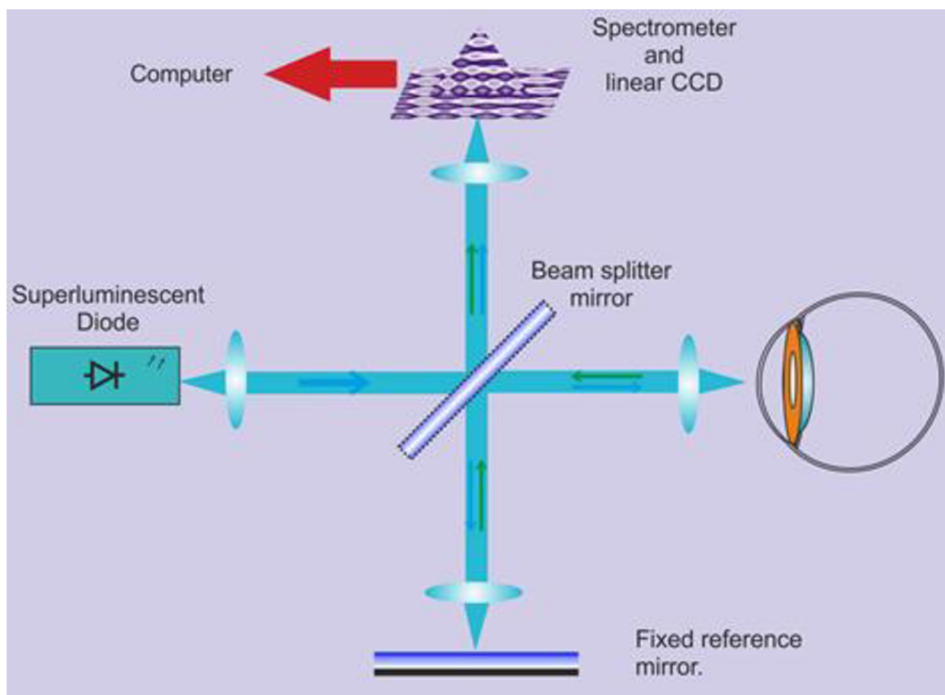
Figure 10: Spectral domain OCT working principle [55]

The most important advantage of this technology compared with TD-OCT is the increased scanning speed, which is 100 times faster than TD-OCT and acquires 40,000 A-scans per second. It improves the image quality (higher resolution), better signal-to-noise ratio, and also minimalizes the artifacts from the motion. It allows good axial resolution of 5–10 microns. The axial resolution of OCT image depends also on the band of a light source of the low-coherence light. Commercial OCT systems use light source with wavelength about either 800–900 nm [47,56] or 1310 nm.

SD-OCT serves as competent and sensitive examination. Captured images are reproducible process of acquisition is simple and fast. The introduction of SD-OCT has extremely extended the diagnostic potential of OCT and offers better chance of observing a disease. The instrument acquired B-scans in fast succession from the top to the bottom and

constructs a 3D map by B-scans aligning. The accuracy of the map depends strongly on the speed of scan acquisition [54].

3.2.1 The principle of the work

Figure 11 views the optical scheme of the imaging probe. The FC/APC fiber output is accumulated and routed to a beam splitter cube where the light beam is divided into a reference beam and a sample beam. This configuration is similar to a Michelson Interferometer. The sample beam hits two galvanometer actuated mirrors for scanning in two axes. Then, it is focused into the sample by the scan objective. Finally the scan objective collects backscattered and backreflected light, from the sample, which finally moves back to the fiber. The light which was reflected into the reference arm is retro-reflected back into the fiber [57].
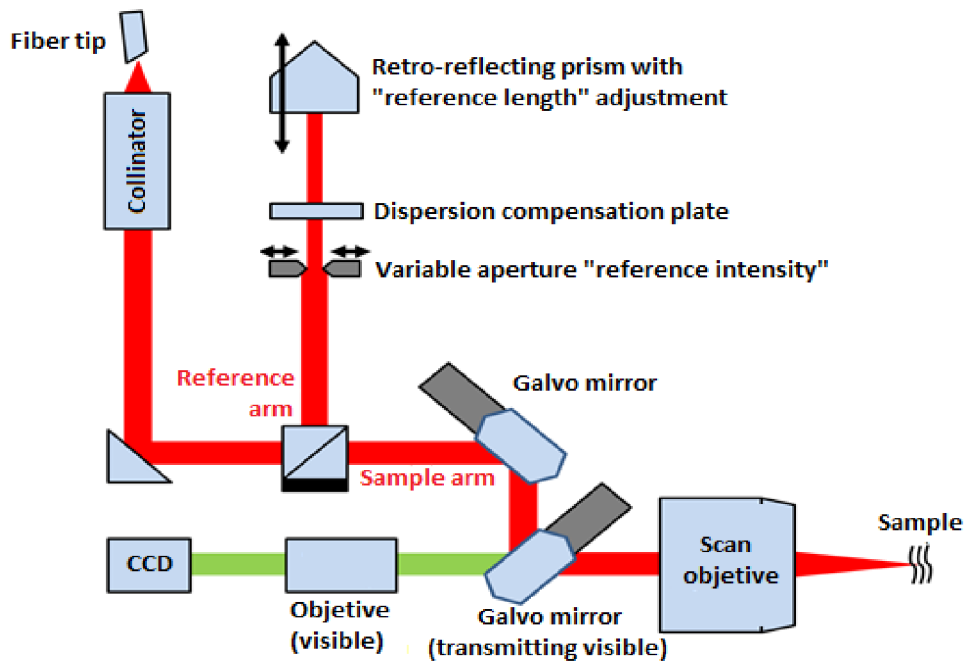
Figure 11: Optical layout of image probe [57]

3.3 Improving of OCT contrast

Possibility of improving a quality of OCT images in tissues has been studying only in recent years. The contrast in OCT images is often limited, especially if pathological tissue is morphologically or optically similar to normal tissue. Therefore, enhancement of OCT contrast has a potential to offer more detailed *in vivo* information and to improve the diagnosis. The different contrast agents were examined for purpose of OCT contrast enhancement. A molecular contrast can be provided by exogenous contrast agents. Also the air microbubbles have been used to improve the intensity of backscattered light from the tissues [13]. NIR dyes,

which are spectrally active have been used as contrast agents for enhancing of contrast in OCT [58].

The nanoparticles consisting from a dielectric (silica) core coated by an ultrathin shell of gold seem to be the most perspective for contrasting OCT images of tissues. The wavelength of plasmon resonances of SiO_2/Au core/shell nanoparticles is situated in the NIR region as well as the operating wavelength of OCT. By varying the dimensions of silica core and gold shell, what was explored [22], the single-particle plasmon resonance and scattering/absorption properties can be spectrally tuned. Therefore, the nanoparticles can be systematically fabricated depending on their planned using. The backscattering with a low absorption is necessary in OCT imaging, while a high absorption is essential in photothermal therapy [13,59].
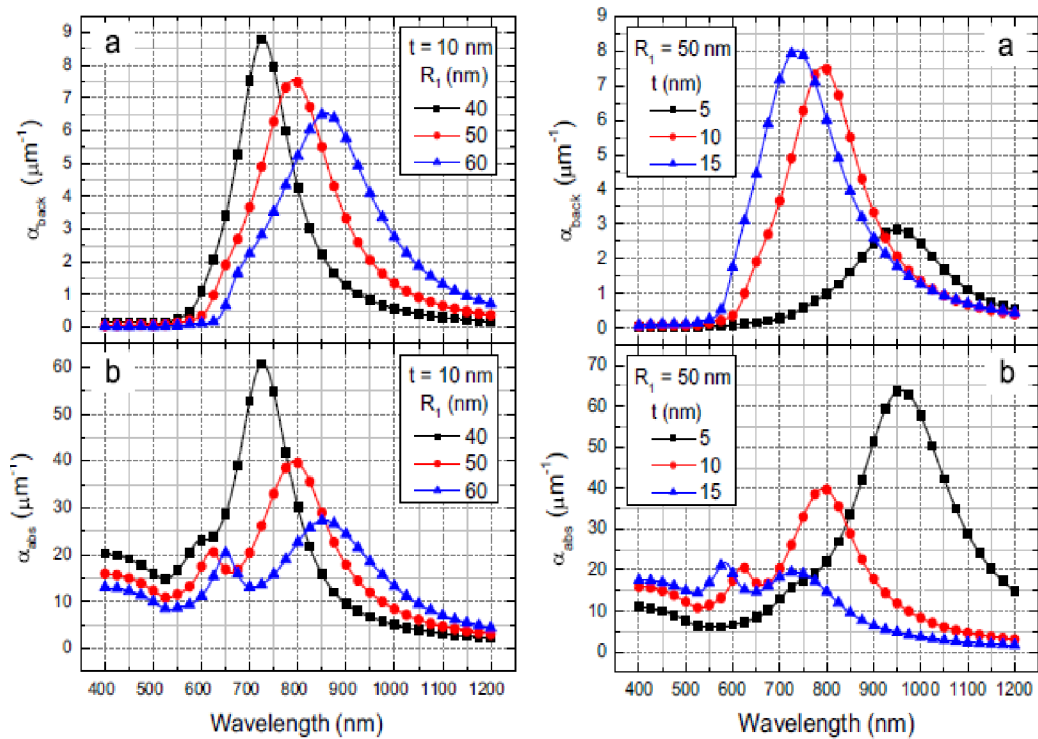
Figure 12: Effect of core radius (R1) on the spectrum of volume scattering coefficient (α_{back}) (a, left); on the spectra of volume absorption coefficient (α_{abs}) of SiO_2/Au nanoparticles with shell thickness (t) (b, left); Effect of shell thickness (t) on the spectra of volume scattering coefficient (α_{back}) (a, right); volume absorption coefficient (α_{abs}) of SiO_2/Au nanoparticles with core radius (R1) (b, right) [22]

Graphs in *Figure 12* show the effect of range of SiO_2 core diameters with invariable thickness of 10 nm gold shell (left) and range effect of gold shell thickness with core size 50 nm (right) of SiO_2/Au nanoparticles, on the spectra of backscattering/absorption coefficients. Depending on the results from graph, nanoparticles exhibit resonance scattering and absorption. Absorption coefficient is presented as two peaks in the spectrum of the graph. The

peak with the longer wavelength responds to the plasmon resonance of dipole and the peak with the shorter wavelength responds to the plasmon resonance of quadrupole. With the increasing radius of core, the position of the backscattering resonance peak red-shifts (727–858 nm) and its intensity decreases. The position of absorption peak of dipole also red-shifts (727–855 nm) and the intensity of this dipole absorption peak decreases. However with the increasing thickness of the shell, the position of backscattering peak blue-shifts (949–736 nm) and the intensity of this peak increases. The intensity of the dipole absorption resonance peak decreases and the position of the peak blue-shifts (959–732 nm). From these results, it is clear that the optical resonance of nanoparticles can be systematically tuned in the visible and NIR regions, by varying the relative dimension of the SiO_2 core and thickness of gold shell [22].

It was also studied the effect of nanoparticle core size and shell thickness on the enhancement of signal by SiO_2/Au nanoparticles in OCT imaging at wavelength 1310 nm. *Figure 13* displays the graph of enhancement of intensities by SiO2/Au nanoparticles with different sizes of cores and shells versus backscattering coefficients predicted for each size of nanoparticles. Data points are labeled in nanometers and show the core diameter/shell thickness. Increases in the size of cores from 126 to 291 nm as well as thickness of shell over the range of 8 to 25 nm produced an increase in OCT signal intensity (from 19 to 28 dB).
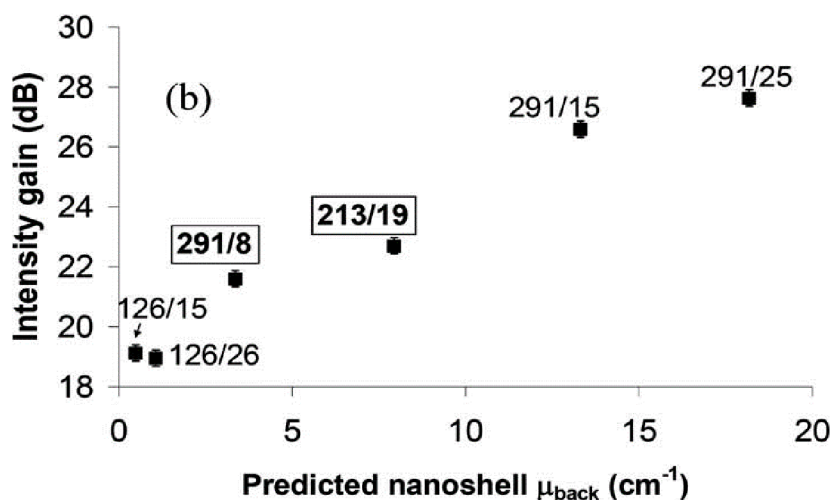
Figure 13: The intensity gain values for nanoparticles with different sizes of cores and shells, added to water, versus the backscattering coefficients (μ_{back}) predicted for each size of nanoparticles [13]

Nanoparticles with greater cores (over 200 nm) and shell thickness greater than 15 nm produced higher backscattering and consequently gained greater intensity. Furthermore, by increasing the shell thickness over 15 nm, absorption efficiencies decrease considerably. Examined nanoparticles with the biggest core and smallest shell (291/8 core/shell) produced a smaller signal than nanoparticles with smaller core and bigger shell (213/19 core/shell). The

291/25 core/shell nanoparticles produced the greatest signal [13]. On these bases, SiO_2/Au nanoparticles with these sizes of core and shell were fabricated.

3.4 OCT testing

Recently, the SiO_2/Au core/shell nanoparticles have been also used as effective contrast agents for OCT imaging in animals [59,60] and tissue phantoms [59]. The SiO_2/Au nanoparticles with 150 nm core and 25 nm shell were analyzed as contrast agents for OCT system in agar biotissue phantoms and rabbit skin. The penetration of nanoparticles into the tissue phantom increased the intensity of the OCT signal in image; concretely it increased the brightness of the areas corresponding to the presence of those nanoparticles.

The contrast enhancement using gold nanoshells is shown in *Figure 14* [59]. There was high concentration of nanoparticles in the upper layer of phantom as can be seen in the middle. Penetration speed of nanoparticles influences the thickness of the bright layer [59]. The OCT system used in this study has operating wavelength 900 nm. Nanoparticles have the maximum backscattering in 850–950 nm.
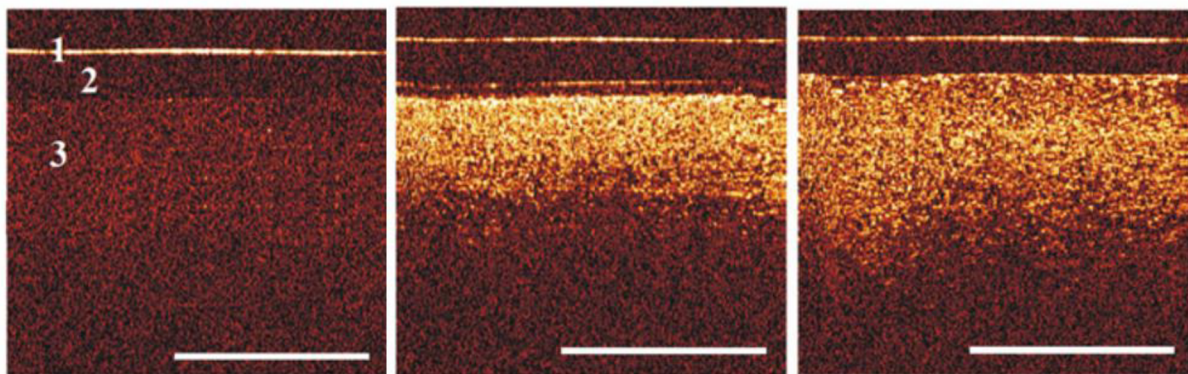
Figure 14: OCT images of the agar biotissue phantom at concentration of agar 0.2 %; before application of nanoparticles (left), 60 min after application (middle), 150 min after application (right) [59]

Application of nanoparticles into the rabbit skin offered also notably higher contrast of the borders between the areas without and with nanoparticles. OCT signal was increased in superficial layer of the skin, also between superficial and deep dermis. Furthermore, the authors found the enhanced contrast of hair follicles and glands, what is illustrated in *Figure 15* [59]. This enhancement of contrast resulted in the increasing of brightness of the skin layers in 30 min after the application. After 180 minutes, OCT image became more obvious in the contrast between the upper (superficial) and deeper layers of skin. Also the borders between these layers became more distinct. Effect of nanoparticles application lasted up to 24 hours [59].
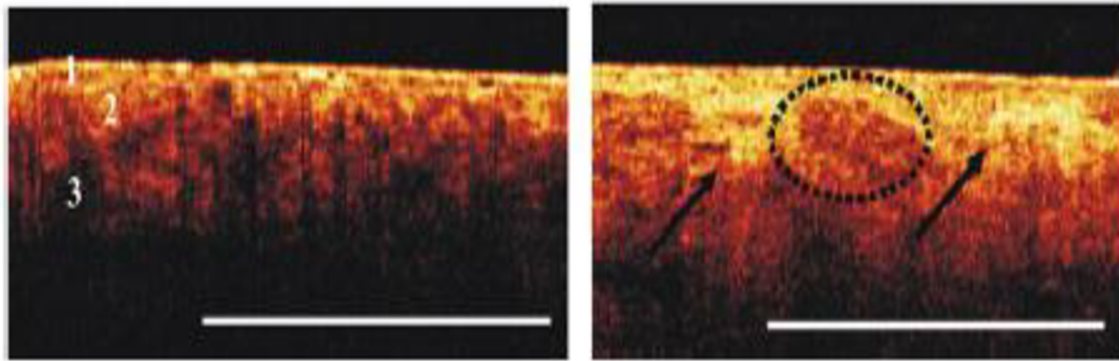
Figure 15: OCT image of the histology of the rabbit skin; before application of nanoparticles (left), 180 min after application (right) [59]

The potential of SiO_2/Au nanoparticles was examined in the cancer imaging. *Figure 16* represents OCT image of normal skin and tumor tissue of mice [60]. The nanoparticles with 120 nm silica core and 12 nm gold shell were systematically injected into these tissues. The surface of nanoparticles was before application modified with polyethylene glycol (PEG) to enhance circulation times in the body and reduce immune reaction *in vivo*. Nanoparticles were injected intravenously and they were accumulated in the tumor tissue. There was high accumulation of nanoparticles inside the tumor tissue, what significantly increased the scattering in NIR spectrum in the tumor. It enhanced the OCT contrast in comparing with normal tissue where was not observed so high increase. Maximum backscattering of used nanoparticles was in 800 nm what corresponds to the operating wavelength (808 nm) of OCT system in this study. OCT images were taken after 20 hours of nanoparticles circulation [60].
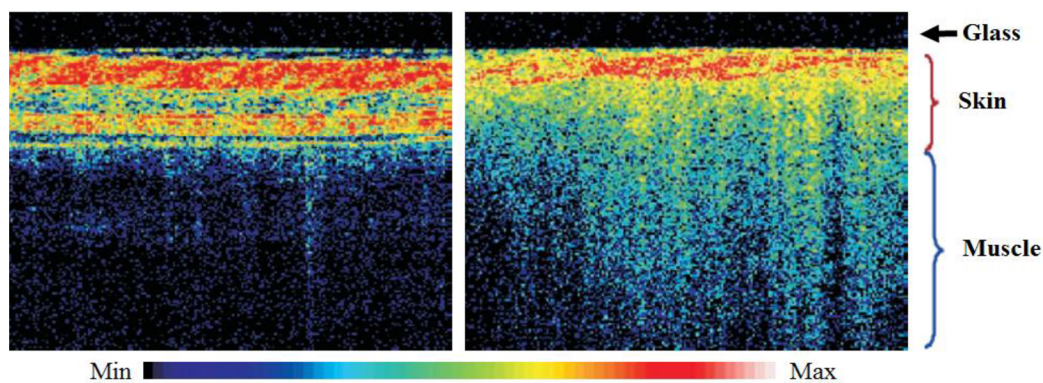
Figure 16: OCT images of tissue areas of mice injected with SiO_2/Au nanoparticles in normal skin and muscle(left); in tumor (right) [60]

4 Characterization methods of nanoparticles

To characterization the properties of nanoparticles and to their measurement can be employed many different experimental techniques. There can be measured size, concentration, surface charge of nanoparticles, *etc*. The majority of techniques are based on the light analysis. The most commonly used techniques are described below.

4.1 Scanning electron microscopy (SEM)

The Scanning electron microscopy is a technique to produce high-resolution imaging of sample surfaces. SEM scans the sample with a high energy beam of electrons and produces the magnified image (>100 000x) [61].

Beam of incident electrons is generated in an electron column. Electrons are focused to beam by a series of lenses. The beam of electrons passes through the lenses and apertures, which deflect the beam vertically and horizontally and hit the sample surface. Scanning coils, above the objective lens, control the position of the electron beam on the sample and allow to scan this beam over the surface of the sample. This focused high energy beam is scanned and at the sample surface is generated signal. Signal, produced from the interaction of electrons with the atoms of the sample, reveals information about the morphology of the sample, and about its chemical and crystalline composition. Detectors detect and intensify the signal. Then, the signal is displayed such as a distribution map of the intensity of the signal which was emitted from the scanned area of the sample. The SEM column and the sample chamber are placed in the vacuum (10^{-5} to 10^{-7}Torr), where are done high-resolutions images with the chamber. This vacuum is necessary because of freely moving of electrons from the electron beam source to the sample and finally to the detectors [61,62].

Produced signal of SEM includes the signal from secondary electrons (it produces high-resolution imaging), from backscattered electrons (BSE that produce SEM image), signal from diffracted backscattered electrons (EBSD that determines crystal structure) and characteristic X-rays (elemental analysis). These signals can be produced on the basis of interaction of electron beam with the inside of sample, where the electrons were penetrating after their hitting of sample surface [63].

Secondary electrons are used for showing morphology and topography of sample and provide very high-resolution images of the sample surface. Backscattered electrons come from the sample and illustrate a contrast in the composition of multiphase samples. The image contrast here is provided as a function of elemental composition and surface topography. Characteristic X-rays are generated by inelastic collisions of the incident electrons with the electrons in discrete atomic orbital of the sample. This imaging mode can identify the elemental composition of the sample by energy dispersive X-ray spectroscopy (EDX) [62,63].
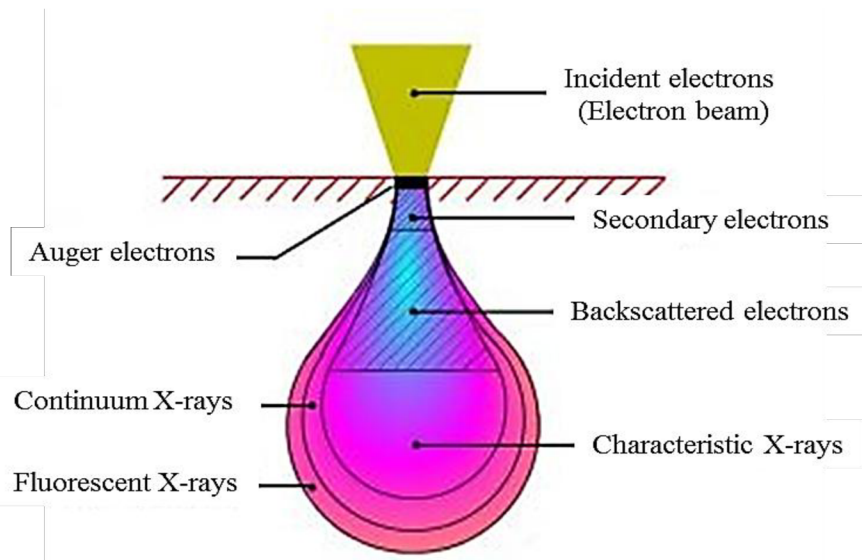
Figure 17: Electron beam interaction diagram of SEM [62]

4.2 Ultraviolet-visible spectroscopy (UV-Vis)

UV-Vis spectroscopy is a technique which quantifies the absorbed and reflected light by a sample. This method uses the electromagnetic spectrum of shorter wavelength, in the visible (400–700 nm) and adjacent spectral region (200–400 nm), which have higher energy radiation. Spectroscopy uses as a light source a halogen lamp and a deuterium lamp, which in combination can offer these visible and UV lights. A monochromator then selects the concrete wavelength of electromagnetic spectrum and directs it into the sample [64].

After interaction of the sample with incident light, it occurs an electronic transition of atoms or molecules in the sample. Atoms/molecules absorb the energy from the light and they are excited from a low energy state to the higher excited state. This transition is the base principle of UV-Vis spectroscopy. Emitted wavelength then corresponds to the level of energy which excited electrons to the higher molecular orbital (excited state).Absorption of the light, as a function of wavelength, gives information about that transition. The light which is absorbed by the sample is specific for each material and it depends on its chemical structure [64,65].

The fraction of the transmitted light is counted by the Lambert-Beer law. It says that the transmittance is directly proportional to the ratio of transmitted light intensity *(I)* to the intensity of the incident light *(I_0)*. Detector measures the light, which passes through the sample, and records the ratio between the intensities of sample beam and reference beam. Sample beam is directed from the light source to the sample and the intensity of a light is measure before and after its passing through the sample. The reference beam travels directly from the light source to the detector. Computer scans the largest different between these beams and it decides at which wavelength, it was adsorbed the UV light. It works on the principle of finding the big mismatches in the intensities. In the place where the intensity of

sample beam is noticeable weaker than the reference beam, the computer determinates this wavelength as the highest UV absorbance in UV spectrum [64,66].
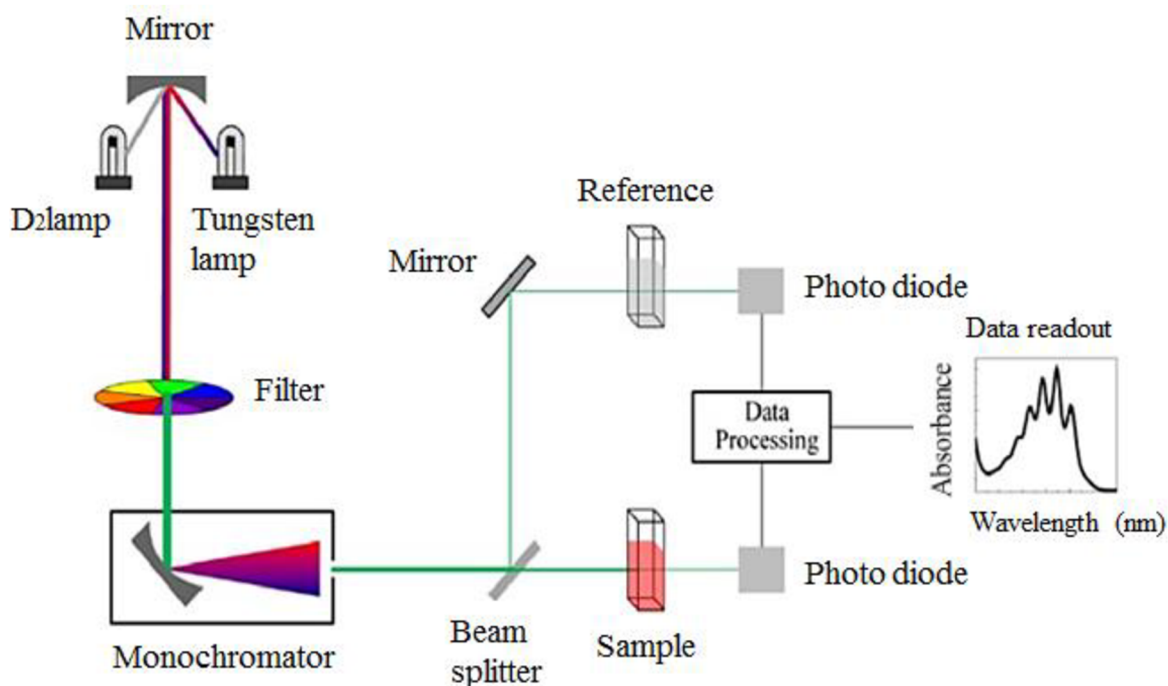
Figure 18: The components and assembly of a UV-Vis spectrophotometer [64]

4.3 Fourier transform-infrared spectroscopy (FT-IR)

FTIR spectroscopy is a molecular spectroscopy technique and chemical analysis method. It uses an infrared radiation which is directed through the sample. Some of this radiation is transmitted by the sample and some is adsorbed. The resulting spectrum performs a molecular absorption of IR radiation by the sample versus wavelength. Concrete absorption bands can be used to identify molecular structures and components. After IR irradiation of molecules in the sample, absorbed radiation excites the molecules to vibrational excited states. The wavelengths of the absorbed light by the molecules are characteristic for molecular structure of the sample [67,68].

This technique is useful for various types of analysis. It can resolve the number of components in a mixture, or determine a consistency of the sample. FT-IR can also identify unknown materials, where the unknown infrared absorption spectrum is compared with the spectrum from a known measured material or with the spectrum which is in database. In the spectrum, it is compared the identity of components in the sample. Typical absorption bands are in the range 4000–1500 wavenumbers. The region in range 1500–400 wavenumbers is known as the fingerprint, where absorption bands are highly specific to each material and no two molecular structures have the same IR spectrum in this region [67,68].

The FTIR spectrometry employs optical device interferometer to produce the wavelengths from broadband infrared frequencies. The intensity of a light (reflected or

transmitted) is recorded by a detector, as a function of light wavelength. Majority of interferometers have a beam splitter, a stationary mirror, and a moving mirror. The light from infrared source is collimated and directed to a beam splitter. That divides the incomings beam into two optical beams and transmits one beam towards the fixed mirror and another beam reflects towards the moving mirror. Both mirrors reflect the IR light back to the beam splitter and light passes to the sample. The result signal (light) leaving the beam splitter and which is directed to the sample is the interference of both beams. Finally the beam passes to the detector. The raw data, which are result signal obtained from detector are called and interferogram. The result signal must be analyzed with a computer, via technique called Fourier transformation. That converts the raw data from detector into the actual spectrum [69].
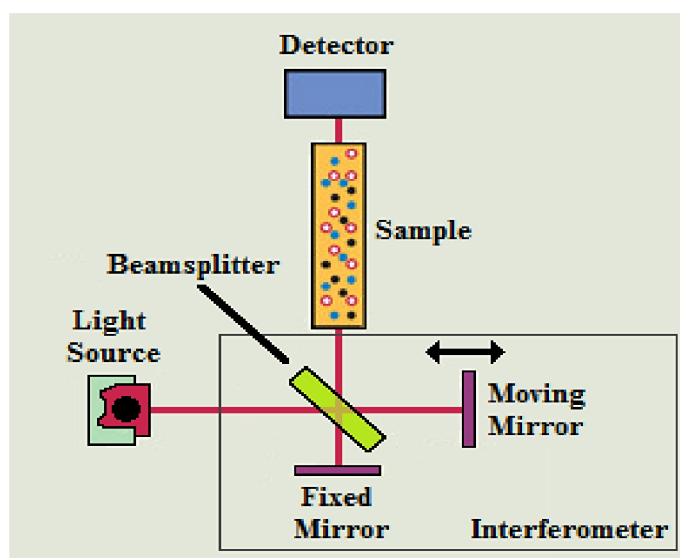
Figure 19: Schematic diagram for FT-IR

4.4 Dynamic light scattering (DLS)

DLS technique is used for measuring the size and size distribution of molecules and particles. Typical applications are characterization of proteins, emulsions, molecules and particle which are dispersed in a liquid. It is possible to determine the size down to 1 nm, typically in the submicron region.

The particles in sample are illuminated by a laser beam and they scatter this light. Analysis of the variation in the scattered light gives information about the particles. All molecules in solution undergo Brownian motion. This motion is related to the detector and there is created constructive or destructive interference which produces a change in the intensity of light. DLS measures these intensities as a function of time. As the time scale of the intensity of light is measured, it is possible to obtain the information about average size or size distribution, and dispersity of elements in solution. Rate of the intensity changes is directly related to the velocity of the Brownian motion of the particles. With the larger

particles, the motion will be slower. Smaller particles will move more rapidly. The velocity of the motion also depends on the temperature or on the viscosity of the solvent. If the temperature in the sample is not stable, convention currents can cause random movements of the particles and obtained results will be incorrect [70,71].

Fast photon detector of the instrument measures a fluctuation of scattered intensity at a known scattering angle. Depending on the angle of scattering, the intensities of scattering are different for the various sizes of particles. Each size of particle has different optimal angle of detection. However, some DLS instruments have possibility to measure only at a fixed angle, what is obviously either at a 90° (right angle) or 173° (back angle) scattering angle. That delivers the mean size of particles only in a limited size range. This measurement can yield good results only for certain particles. DLS instruments which offer measurements at several scattering angles (multi-angle) perform a high quality of analysis. Therefore, it can be determined the full distribution of particle sizes in the polydisperse samples [72].
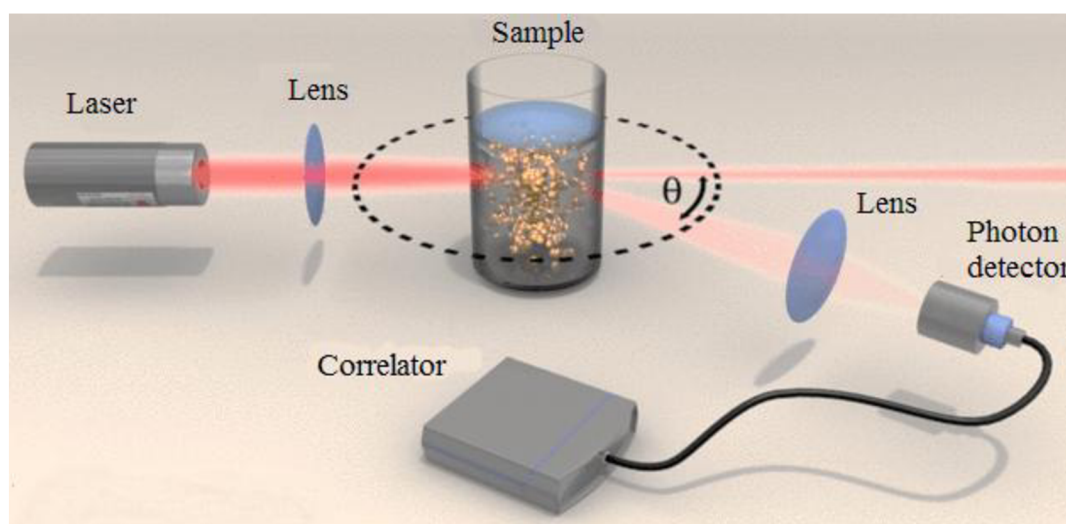
Figure 20: Schema of DLS principle [72]

4.5 Near-infrared spectroscopy (NIRS)

NIRS is an absorption spectroscopic technique. The sample is irradiated with the polychromatic source of light, from which the sample absorbs only frequencies which correspond to its molecular vibrational transitions. The near-infrared (NIR) spectrometers are identical to spectrometers working in another region of electromagnetic spectrum. The NIR region is located in the wavelength range 780–2500 nm. In this area absorption bands correspond to the molecular overtones (up to 1800 nm) and to the combination bands (over 1800 nm) of the investigated molecules. Combination bands are typically located at lower energies in comparing with overtones. They are the sum of several fundamental bands. Combination bands with hydrogen (O-H, N-H, C-H*, etc.*) are strong NIR absorbers and dominate the spectrum [73,74].

In the NIR spectrum it is often difficult to assign bands of the overtone and combination bands to the specific chemical components because they are typically very broad. Therefore there can be used multivariate calibration technique with multiple wavelength to obtain the needed chemical information [73,74].

There are 2 types NIR spectrometers depending on the selection of wavelengths. The first type works in the region of discrete wavelength. For selection of wavelengths it uses filters of the light source, which allow pass broad bands of wavelength. Another possibility is using of light-emitting diode (LED) which emit only narrow wavelength bands. Second type of NIT spectrometer, for whole-spectrum NIR, they use to contain a diffraction grafting or they can be type of Fourier transform NIR (FT-NIR).This type of spectrometers is more flexible [75].

5 Experimental section

The following experimental part is focused on the synthesis of SiO$_2$/Au core/shell nanoparticles and on the investigation of the influence of this type of nanoparticles on the enhancement of optical coherence tomography (OCT) signal.

Synthesis of SiO$_2$/Au core/shell nanoparticles consists of molecular self-assembly with colloid chemistry in aqueous solution. Silica cores were fabricated by Stöber method. Consequently, they were functionalized with 3-aminopropyltriethoxysilane (APTES). For the gold shell, small colloidal gold nanoparticles were synthesized according to Duff process.

After synthesis, the properties of produced SiO$_2$/Au core/shell nanoparticles were analyzed, such as their morphology, complex structure and optical properties. Finally the OCT was performed in 930 nm in water to which SiO$_2$/Au core/shell nanoparticles were added. The effect of nanoparticles concentration on signal enhancement was characterized.

5.1 Material (reagents)

All chemicals used in this work are shown in *Table 1*. Can well as their purity, CAS number and supplier.

Table 1: List of chemicals used in this work

Product name	Purity	CAS Number	Producer
Ammonia solution	25 % for analysis	1336-21-6	MERCK
Ethyl alcohol absolute (EtOH)	p.a.	64-17-5	PENTA
Formaldehyde 36-38 %	p.a.	50-00-0	PENTA
Gold (III) chloride trihydrate	≥ 99.9 %	16961-25-4	Sigma-Aldrich
Isopropyl alcohol (IPA)	p.a.	67-63-0	PENTA
Millipore water Milli-Q	-	-	HACH
Potassium carbonate anhydrous	pure	584-08-7	PENTA
Sodium hydroxide	p.a.	1310-73-2	PENTA
Tetraethyl orthosilicate (TEOS)	for synthesis	78-10-4	MERCK
Tetrakis (hydroxymethyl) phosphonium chloride (THPC)	80 % in H$_2$O	124-64-1	Sigma-Aldrich
3-aminopropyltriethoxysilane (APTES)	for synthesis	919-30-2	MERCK

Also the commercial samples of nanoparticles were analyzed in OCT measurement. First samples, silica/gold core/shell nanoparticles, were purchased from NanoComposix, Czech Republic. The purchased nanoparticles had the same composition and similar sizes as synthetized nanoparticles. The silica core diameter of nanoparticles was 200 nm and the gold shell thickness was around 20 nm. Nanoparticles were placed in Millipore water. Maximum of the absorption spectra (plasmon resonance peak) of tested nanoparticles was at 980 nm what corresponded to the central wavelength of OCT system which was used for

measurements (930 nm). The SEM image and UV-Vis spectrum of commercial nanoparticles are shown in *Figure 21*.
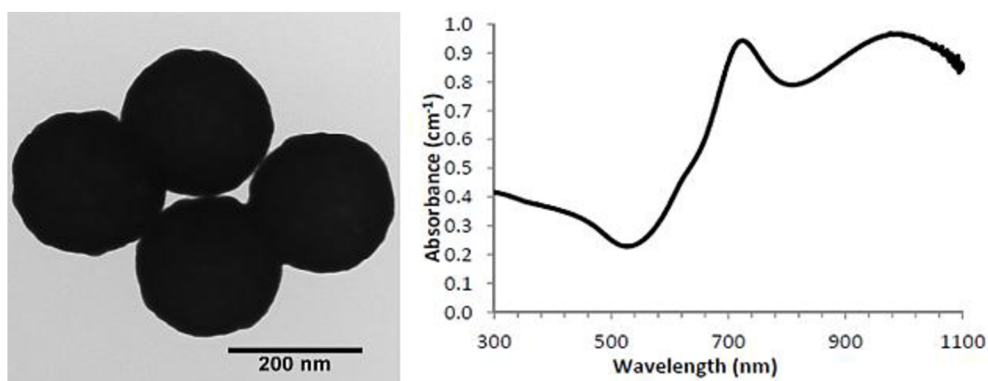
Figure 21: SEM image of SiO₂/Au commercial nanoparticle (left); UV-Vis spectrum of
SiO₂/Au commercial nanoparticles (right) [76]

Second samples, gold nanorods were purchased from Nanopartz, Loveland, Colorado. Tested nanorods had diameters 10 nm and 25 nm and lengths 102 nm and 245 nm. The SPR corresponding peaks was at 1400 nm for both samples. It corresponded to the central wavelength of OCT system (1300 nm). The TEM image and UV-Vis spectrum of gold nanorods with the size 25/245 nm (25-1400) is shown in *Figure 22*.
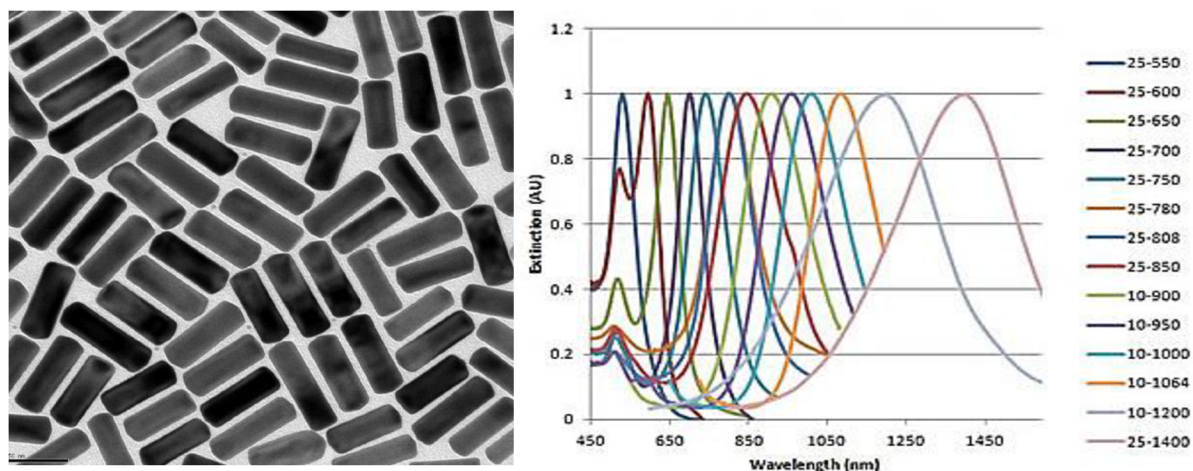
Figure 22: TEM image of commercial gold nanorods with the size 25/245 nm (left); UV-Vis
spectrum of commercial gold nanorods with the size 25/245 nm – pale violet color (right) [77]

5.2 Apparatus used in experimental work

Morphology of the nanoparticles was analyzed by scanning electron microscopy (SEM). Ultraviolet visible (UV–Vis) spectroscopy was used for examination of optical properties. Complex structure of the core–shell nanoparticles was analyzed by infrared Fourier transform spectroscopy (FT-IR). Size distribution profile of nanoparticles in the

sample was obtained by Dynamic light scattering (DLS). The optical coherence tomography (OCT) was used for testing signal enhancement by SiO_2/Au nanoparticles.

5.2.1 pH meter

For pH measurement of the sample was used pH meter Cyberscan pc 6500, Eutech instruments. That was dipped into the sample containing nanoparticles for tens of seconds in the process of measurement.

5.2.2 SEM

The shape and size of nanoparticles were analyzed by scanning electron microscope Tescan FE–SEM MIRA II LMU (from The Faculty of Electrical Engineering and Communication, BUT). It was used magnification 7000–25000 kx. The samples were dropped onto silicon wafer and any residual ethanol from samples was vaporized before analysis.

5.2.3 FTIR

The FTIR data were collected using spectrometer Nicolet iS10 FT–IR (from The Faculty of Chemistry, BUT). Spectrum was recorded in the range of 400–4000 cm^{-1}. Main idea was detection of NH bond in the absorption spectrum. This bond shows the presence of amine grafted silica particles in SiO_2/Au nanoparticles. It represents the successful functionalization result of silica core, what is principle for sufficient and uniform binding of the gold colloid. In the evaluation of the results was taken into the consideration following graph shown in *Figure 23* [78].
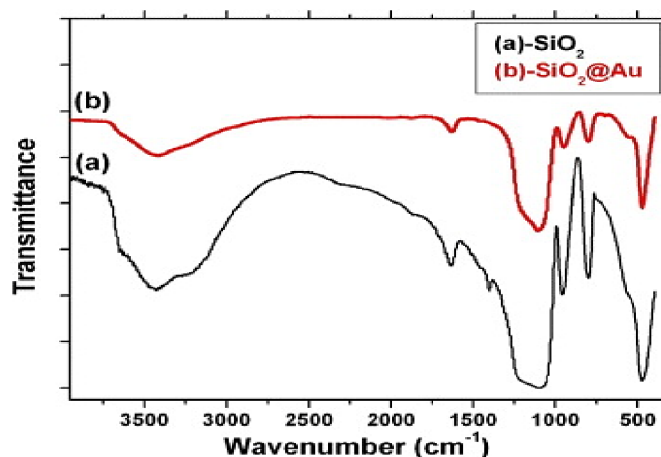
Figure 23: FTIR spectra of a) SiO₂; b) SiO₂/Au core/shell nanoparticles [78]

5.2.4 Uv–Vis

To analyze the optical properties was used ultraviolet visible (UV–Vis) spectroscopy. Optical absorption spectra of the samples were measured using a spectrophotometer Specord 210, Analytik Jena AG (from Mendel University, Brno).
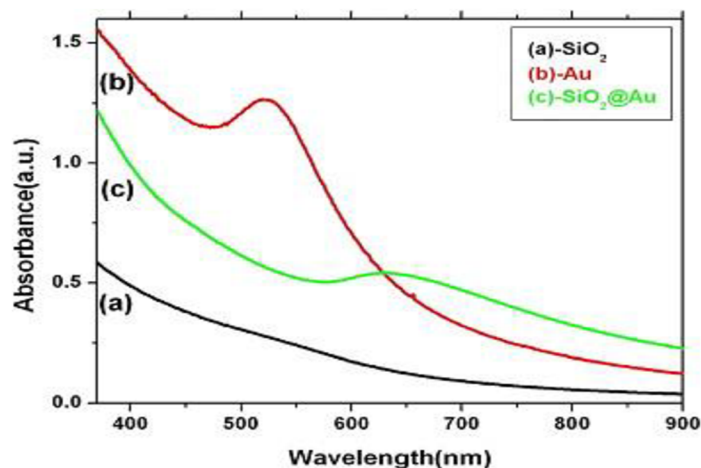
Figure 24: Optical absorption (UV–Vis) of a) SiO$_2$ nanoparticles; b) Au nanoparticles; c) SiO$_2$/Au core/shell nanoparticles [78]

UV–Vis analyzes were performed in the wavelength range of 400–900 nm. All samples were dispersed in Millipore water and placed in the spectrophotometric cuvettes during the analysis. The results of absorption spectra should approximate to the spectrum in the graph, which is shown in *Figure 24 [78].*

5.2.5 DLS

To determine the size distribution (number, volume an intensity distribution) profile of nanoparticles was used Zetasizer Nano ZS (ZEN 3500), Malvern Instruments Ltd (from Mendel University, Brno).During the measurement, all samples were dispersed in Millipore water and placed in cuvettes in volume 50 μL. DLS analysis was carried out at 23°C.

5.2.6 NIRS

For measurement near-infrared spectrum of gold nanorods from Nanopartz was used The Sol 1.7 Cooled linear TE InGaAs array spectrometer, BWTEK with fiber optic combined light source LS 10, SAFIBRA (from Faculty of Electrical engineering and Communication, BUT). Spectrum was recorded in the wavelength range 1050–1450 nm. Samples were placed in spectrophotometric cuvettes.

5.2.7 OCT

Thorlabs OCS1300SS, Swept Source OCT system (from Faculty of Electrical engineering and Communication, BUT) was utilized in this work for testing of bare gold nanorods from Nanopartz. It was analyzed their property to enhance the OCT signal. Nanorods have SPR peak at 1400 nm what responses to the central wavelength of this system. Central wavelength together with other specifications of system are presented in *Table 2* below [79].

Table 2: Technical specifications of Thorlabs OCS1300SS, Swept Source OCT system [79]

System specifications	
Central wavelength (nm)	1300
Image speed (A-scan line rate) (kHz)	16
Axial resolution air/water (µm)	12 / 9.0
Lateral resolution (µm)	25
Maximum imaging depth (mm)	3
Imaging speed (512 lines/frame) (fps)	25
Maximum pixels per A-scan	512

Thorlabs'hight-sensitivity CALLISTO, Spectral domain OCT system (from The Valencia Nanophotonics Technology Center (NTC), Polytechnic University of Valencia) was used in this work to examine the contrast enhancement of purchased samples gold nanoshells from Nanocomposix. During the investigation, nanoparticles were placed to the Millipore water and the obtained intensity of OCT signal which was achieved by addition of nanoparticles was concerned. The technical specifications of OCT CALLISTO system are displayed in *Table 3* [57].

Table 3: Technical specifications of Thorlabs'hight-sensitivity CALLISTO, Spectral domain OCT system [57]

System specifications	
Central wavelength (nm)	930
Image speed (A-scan line rate) (kHz)	1.2
Axial resolution air/water (µm)	7.0 / 5.3
Lateral resolution (µm)	8
Maximum imaging depth (mm)	1.7
Imaging speed (512 lines/frame) (fps)	2
Maximum pixels per A-scan	512
Sensitivity (dB)	105

This OCT system contains few main components as a base unit, a PC, an imaging probe and a probe stand. Constructed system is illustrated in *Figure 25 [80]*.

Figure 25: Spectral domain OCT system [80]

The base unit beams a light to the application, initializes the spectrometer's camera, and communicates and delivers the measurement data to the PC through a USB connection. The base unit contains super luminescent diode (SLD) light source which is directed to the probe port of the device through a fiber optical device. Reflected and backscattered light from the sample is returned to spectrometer. The central wavelength of the system is 930 nm. The use of near-IR broadband source is a perfect compromise between low scattering losses and sufficient penetration depth. The probe stand provides X-Y scanning for 3D acquisition of data. In the probe, there is integrated a camera, which provides video imaging during the acquisition of OCT data. Imaging probe in OCT is located within interferometer, what eliminates the problems with chromatic and polarization mode dispersion [57,80].
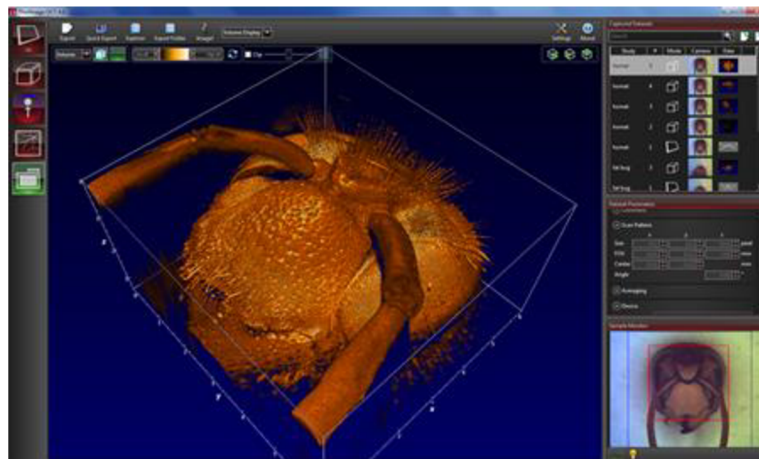
Figure 26: High performance software used in OCT CALLISTO system [80]

The PC is created from all the necessary data acquisition hardware, software, drivers to start imaging upon arrival. The measured data are delivered to the PC through a USB connection. System employs a software development kit (SDK) which is shown in *Figure 26*. The software performs acquisition of data, their processing, scan control, and finally display of OCT images [80].

5.2.7.1 Acquisition mode

There are a few possible different acquisition modes which can be selected for OCT CALLISTO imaging of sample [81]:

- 1D mode (A-scans)
- 2D mode (B-scans)
- 3D mode (Volume scans)
- Doppler mode (Doppler data)
- Speckle variance mode (Speckle variance data)

First 2 acquisitions modes, A-scan and B-scan, were used in this work in process of testing nanoparticles and their enhancement of OCT contrast. 1D mode is a depth profile from the interference of photons which were sent and received back from the sample with photons which were reflected from the reference mirror. A scans are collected in the depth direction at the beam position. This mode is selected in *Figure 27 [81]*.
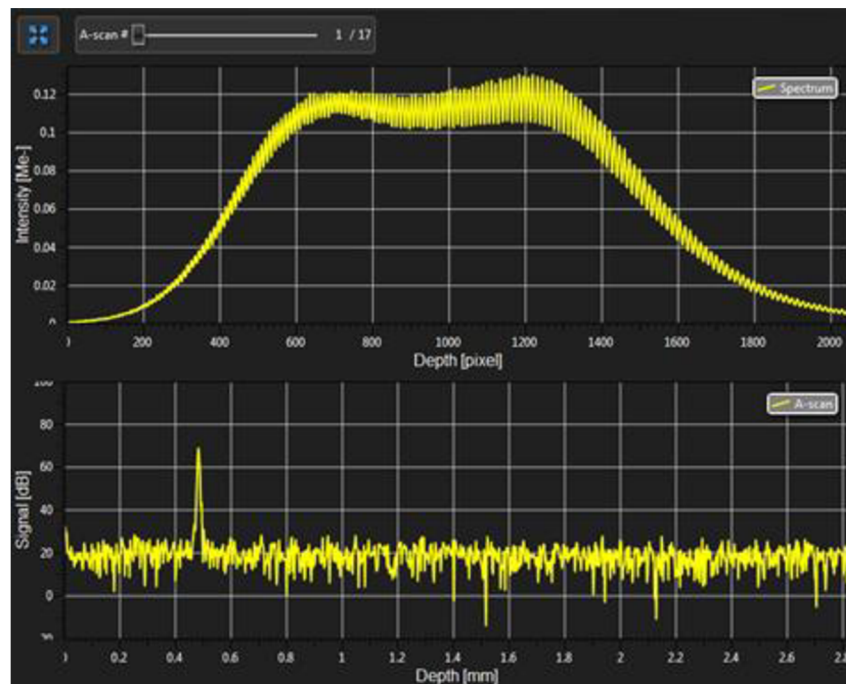
Figure 27: 1D acquisition mode (A-scan) [81]

In 2D mode, one galvanometer mirror is scanning. The probe beam scans in transverse direction whereas A-scans are collected in the depth direction. These A-scans create a 2D cross-sectional OCT image (B scan), which is illustrated in *Figure 28.* OCT images are displayed in real time [81].
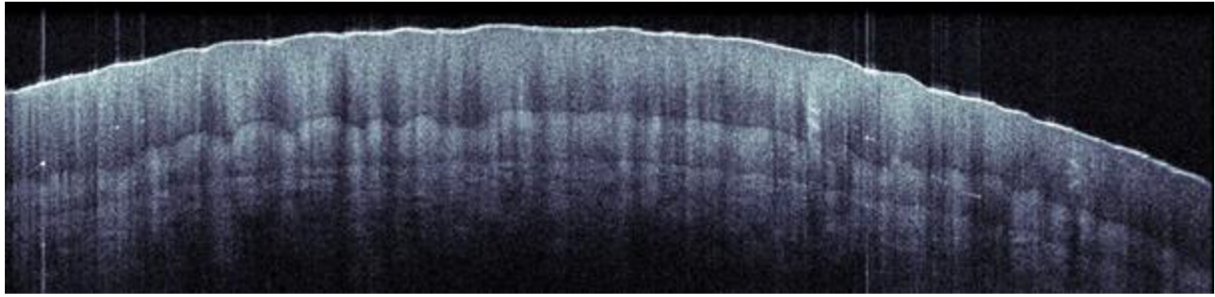
Figure 28: 2D acquisition mode (B-scan) [57]

In 3D mode, there both galvanometer mirrors are scanning, while volume is acquired. The probe beam scans step by step across the sample to collect series of 2D cross-sectional images, which are subsequently processed to create a 3D image. That is shown in *Figure 29*. This mode is suitable for samples with small or no movement since the measurement takes some time depending on the numbers of A-scans per B-scan and B-scans per volume. In the OCT software, 3D datasets can be viewed in all three orthogonal cross-sectional planes independent of the orientation of acquisition. Another alternative of view is volume rendering, what provides a volumetric rendering of the acquired volume dataset [81].
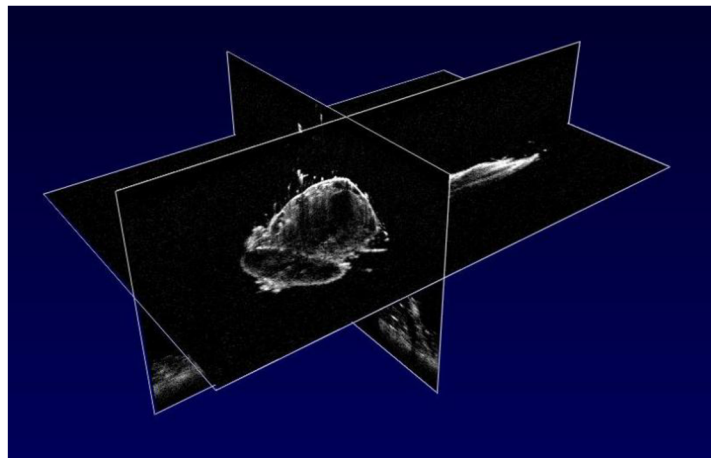
Figure 29: 3D acquisition mode (volume scan) [81]

Doppler mode measures flow velocities of scattering structures. Method uses additional post-processing to extract phase shifts between successive A-scans. Those are averaged to calculate the Doppler frequency shift induced by motion of particle or by flow. Images of Doppler mode are displayed with a color map, which indicates forward flow or backward flow, relative to the OCT beam. These flow velocities have red or blue color scheme, where colors indicate the maximum positive (blue color) or negative (red color) flow velocity in scanning direction. This acquisition mode is possible to see in the following *Figure 30* [81].
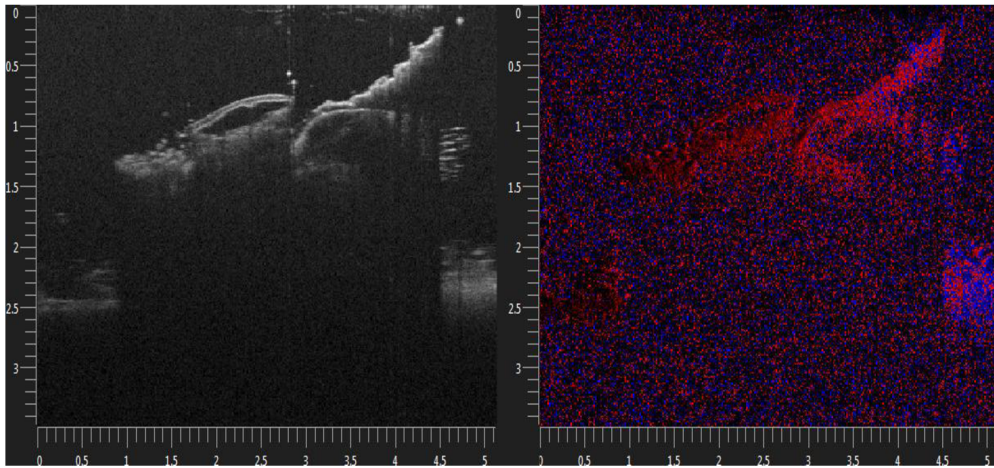
Figure 30: Doppler acquisition mode [81]

Speckle Variance mode uses the variance of speckle noise for angiographic imaging. It shows blood vessel trees without requiring of significant flow of blood and without requiring a specific acquisition speed. The speckle variance data can provide information about morphology. Multimodal pictures can be displayed using the different colors in map *(Figure 31)* [81].
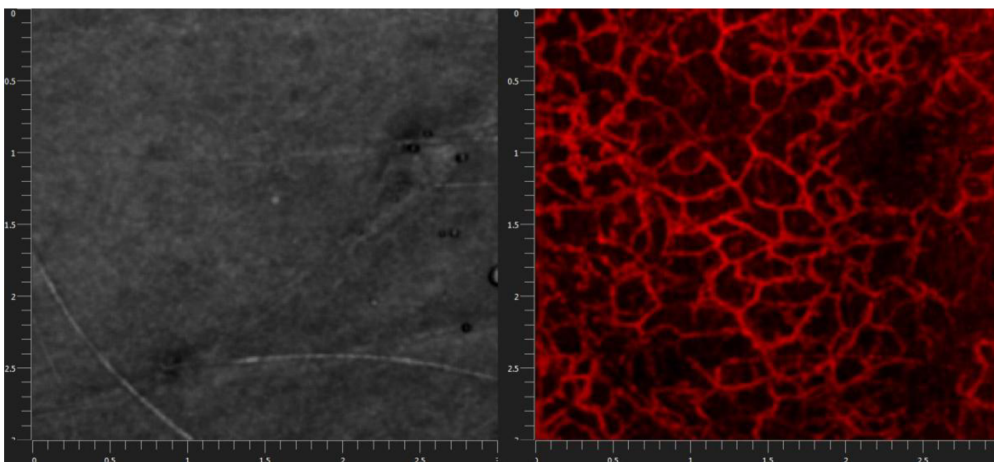
Figure 31: Speckle variance acquisition mode [81]

5.3 Sample preparation

Synthesis of SiO_2/Au core/shell nanoparticles involves the synthesis of silica nanoparticles (cores), the modification of their surfaces by APTES with the resulting amino groups attached on the silica cores, production of colloidal gold nanoparticles in solution, adsorbing of these gold nanoparticles to the amine groups and growth of a gold layer until the complete shell is obtained. This process is illustrated in *Figure 32*.
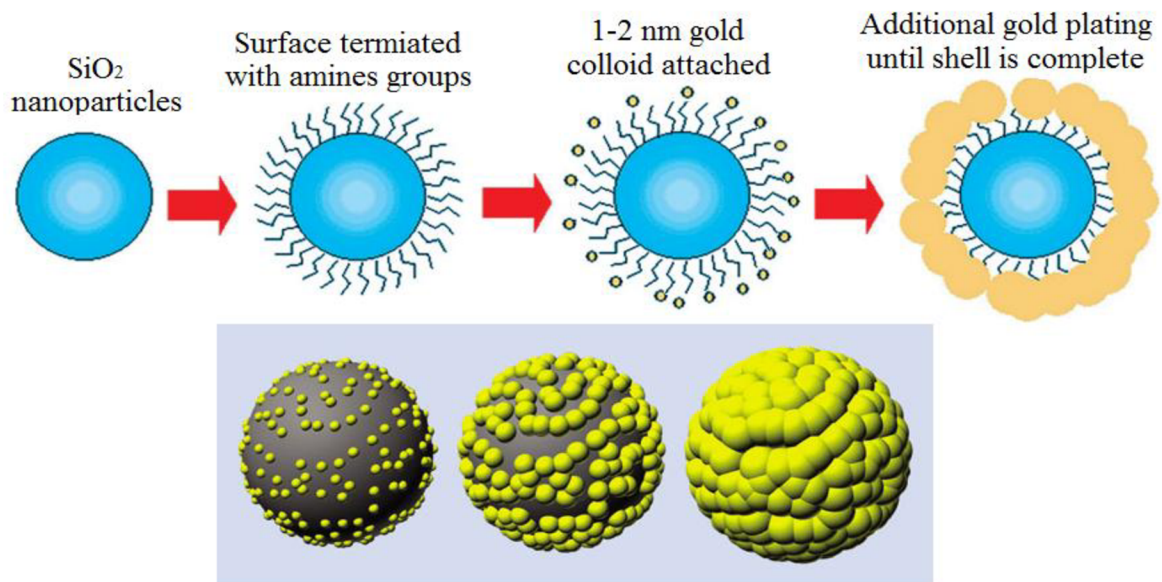
Figure 32: Process of SiO₂/Au core/shell nanoparticle synthesis (up); Growing process of the gold nanoshell on the silica surface (down) [82]

5.3.1 Synthesis of silica nanoparticles

Silica nanoparticles were synthesized by sol–gel process based on the Stöber method. This synthesis includes using TEOS (tetraethyl orthosilicate), alcohol in water and in the presence of organic base (Nh_4OH). It is one of the simplest processes and the most effective for preparing of monodispersed silica nanoparticles. Reaction conditions are controllable and it is not difficult to be carried out.

The main goal of the synthesis was to synthetize the spherical monodispersed silica nanoparticles with the 290 nm size. Agrawal *et at* obtained, that this size of nanoparticle silica core can product a significant increase in OCT signal intensity [13]. In the procedure, ammonia and Millipore water were dissolved in alcohol (ethanol or isopropyl alcohol). The suspension was stirred rapidly (800 rpm) and after 5 minutes a certain amount of TEOS was added drop wise with continuous stirring (600 rpm) overnight. The solution changed from colorless to white in one hour after addition of TEOS. *Table 4* shows the quantity of solvents in the various samples of the silica nanoparticles. The silica nanoparticles were after stirring separated from the suspension by centrifugation at 6000 rpm for 15 minutes and re–suspended in ethanol in 3 cycles of this washing (except the sample *E* which was re–suspended 3 times in Millipore water and 1 time in ethanol). Then, the particles were dried in an oven at 50–60°C overnight and sent for analysis.

Table 4: Quantity of particular solvents in the SiO$_2$ samples, their size and the time of reactions

Sample	EtOH (mL)	IPA (mL)	NH$_4$OH (mL)	H$_2$O Millip. (mL)	TEOS (mL)	Reaction time (hod)
A1	-	73.8	9.8	10.8	5.6	21
A2	70	-	2	25	6	10
A3	74	-	3.14	10	6	20
B1	76.4	-	9.8	10.8	3	22
B2	-	73.8	9.8	10.8	5.6	23
C1	74	-	3.14	10	6	28
C2	-	73.8	7	10.8	4	18
C3	-	73.8	4	10.8	4	22
D1	74	-	3.14	10	5.7	20
D2	-	74	3.14	10	5.7	21
E	148	-	6	20	11	19

5.3.2 Functionalization of silica nanoparticles

Functionalization of silica nanoparticles is one of the crucial steps in the synthesis of SiO$_2$/Au core/shell nanoparticles. Adequate and uniform binding of the gold colloid in the subsequent step is possible only if the surface of SiO$_2$ nanoparticles is coated by hydroxyl groups (OH). These allow a reaction of SiO$_2$ cores with APTES what forms an amine-modified silicon surface which is necessary for subsequent binding of gold colloid. Amine groups are the most important limitation in the spherical shape of the gold nanoparticles [78,83].

Silica nanoparticles were functionalized by APTES. At first they were dispersed as 10 wt % in EtOH (40 mL) under the rapid stirring and placed in the polypropylene flask. Then, APTES (670 µL) was added to the solution under the continuous stirring. The solution was stirred in the night and next day boiled for 2 hours. EtOH was continuously added to the suspension to prevent a total evaporation of the solution during the process of boiling. Finally the functionalized cores were centrifugally separated from the suspension (5000 rpm for 15 minutes) and washed with ethanol 3 times. Finally the particles were dried in the oven at 50–60°C overnight [84]. The volume of APTES in reaction and centrifugal force were modified related to the particle size of synthetized nanoparticles.

Functionalization of silica nanoparticles is very sensitive step. The final modified silica surface depends strongly on temperature of solutions, concentration of APTES, presence of water, time of reaction, and pH [83].

5.3.3 Synthesis of amino–functionalized silica nanoparticles

Other samples, amino–functionalized SiO_2 nanoparticles, were synthesized by synchronized hydrolysis of TEOS and APTES in the presence of ammonia and ethanol (also water was used in some samples) [85,86].

Ammonia was dissolved in ethanol (together with Millipore water). The suspension was stirred rapidly (800 rpm). After 5-10 minutes of stirring, TEOS was added drop wise with continuous stirring (600 rpm). The solutions of silica nanoparticles were continuously reacted by adding APTES to the solutions to produce amino–functionalized SiO_2 nanoparticles. This process was based on the modification of Stöber method [85]. *Table 5* shows the various amounts of reagents in the samples and the time of reactions. The functionalized silica nanoparticles were washed in 3 cycles of centrifugation and re–dispersion in ethanol (sample Z in water) at 6000 rpm for 15 minutes each times to remove all reactants. After washing, the nanoparticles were dried in the oven at 50–60°C overnight.

Table 5: Amounts of reagents in the samples of amino-functionalized SiO_2 nanoparticles and the time of synthesis

Sample	EtOH (mL)	NH₄OH (mL)	H₂O Millip. (mL)	TEOS (mL)	APTES (mL)	Time of reaction (hod)
X	5	0.5	-	0.5	0.005	2
Y	148	6	19	10.5	1	20
Z	150	15	-	15	0.15	18.5

5.3.4 Re–functionalization of <u>amino–functionalized</u> silica nanoparticles

Sample Z was in the previous step washed by water, what could influence the number of OH groups on the silica surface. These hydroxyl groups are necessary in the binding process of amino groups to the silica nanoparticle surface. Therefore, functionalization step was repeated to further improve the quantity of amine groups on the surface in this sample [84]. Also, sample Y was used in this step of re-functionalization. It was employed the same recipe with the same quantity of reagents as in the functionalization of SiO_2 nanoparticles above. After reaction, the nanoparticles were washed in 3 cycles of centrifugation at 6000 rpm for 15 minutes and re–suspension in ethanol. Then, nanoparticles were dried in the oven at 50–60°C overnight.

5.3.5 Preparation of colloidal gold nanoparticles

The gold colloid is produced separately from reduction of $HAuCl_4$ by alkaline THPC, according to the procedure of Duff. The solution of gold colloid has size 1–2 nm in diameter. 4.8 mL NaOH (1M) and 16 mL of THPC stock solution (prepared by adding 400 μL of 80 % THPC in water to 33 mL of Millipore water) were added to 720 mL of Millipore water. After 5–10 minutes of continuous stirring, 27 mL of 1 wt % aqueous $HAuCl_4$ was added quickly.

Solution was stirred for 30 minutes and in this time the color of solution was changed from colorless to dark reddish brown what indicates the formation of the THPC–gold nanoparticles [60,78,84]

Gold colloid was stored in amber bottle in the fridge for 2 weeks. After this time, the colloid was 20 times concentrated through the rotary evaporator (Heidolph, Hei–VAP series) to the final volume of 40 mL. During the evaporation, it was set up a temperature 85°C and an initial vacuum pressure under 200 mbar. Used rotation speed was 35 rpm [60].

5.3.6 Preparation of silica–gold core–shell nanoparticles

The concentrated colloid was mixed with SiO_2–APTES nanoparticles dissolved in EtOH. The solution was stirred under a strong vortex for 15 minutes and then allowed to sit for 2 hours. The small gold colloids attached to the larger SiO_2/APTES–functionalized core surface, where they acted as nucleation sites in the subsequent step, growth of the gold nanoshells [78].

Four different groups of SiO_2/APTES/Au samples were prepared. They were synthesized from the samples of functionalized silica nanoparticles E, Y, Z. Different ratios of SiO_2/APTES nanoparticles, EtOH and gold colloid were used in the samples. The quantities of particular reagents are shown in the following *Table 6*.

5.3.7 Growth of the gold nanoshells

SiO_2/APTES/Au nanoparticles were added to the gold ion-plating solution in the growing process of gold shell on the silica core. The plating solution (PS) was made from 25 mg (0.18 mmol) of potassium carbonate (K_2CO_3) dissolved in 100 ml of Millipore water under stirring for 10 minutes. Then 1.5 mL (20 mmol) of a solution 1 % $HAuCL_4$ in water was added. The solution changed the color from transparent yellow to colorless in 30 minutes [78,86]. The thickness of the gold nanoshell can be regulated by the ratio of SiO_2/APTES/Au nanoparticles to gold–plating solution [86]. In the first and last groups of samples, SiO_2/APTES/Au nanoparticles were injected to the fresh rapidly stirred gold PS. In another samples (groups), the solution was stored for 3 days before using in the amber bottle in the fridge. After 15 minutes of stirring, formaldehyde (0.36 mmol) was added to the mixture. Formaldehyde can lead to the aggregation of nanoparticles [87]. The storage of the gold PS should improve the quality of synthetized nanoshells. The highest quality should be obtained after 1-3 days of its storing [84]. The solution changed the color to blue–gray. Blue color is characteristic for nanoshell formation. Finally the nanoparticles were centrifuged (6000 rpm for 15–20 minutes) and redispersed in Millipore water in 4–5 cycles. Particles were dried in the oven at 50–60 °C overnight.

Table 6: The amounts of reagent in SiO₂/APTES/Au synthesis and in the process of growing of gold nanoshells

Samples	Preparation of SiO₂/EtOH/Au		Ratio of mixed solutions (mL)		
	$SiO_2/EtOH$ (1g/10 mL)	Au colloid (mL)	$SiO_2/EtOH/Au$	Gold PS	Formaldehyde
1/ E, Y, Z	0.3	5	0.6	12	0.09
2/ E, Y, Z	3	5	1	8	0.7
3/E, Z	4	11	3	19	0.8
4/E	5	8.5	11.5	101.5	3

6 Results and discussion

6.1 pH

The pH of silica nanoparticles was measured after their synthesis and during the process of their washing by Millipore water. *Table 7* gives the values of pH measurements. Those were moving to neutral values by individual washings.

Table 7: pH values of the sample E after the synthesis before and during the process of washing by water

Washing by H_2O	pH
Before washing	11.45
After 1st washing	10.65
After 2nd washing	10.15
After 3rd washing	9.99

The pH sample was also measured after the process of re-functionalization of silica nanoparticles and in the process of their washing by ethanol. Measurements are shown in *Table 8.* The result values are almost neutral.

Table 8: pH values of the samples Y and Z after their re-functionalization, before and during the process of washing by EtOH

Washing (EtOH)	pH (Y)	pH (Z)
Before washing	11.44	11.56
After 1st washing	10.5	10.21
After 2nd washing	9.7	9.24
After 3rd washing	8.11	8.15

It was obtained that uniform gold nanoparticles can be synthetized to be very near to neutral conditions. Low or high values of pH may reveal the different formation mechanism of gold nanoparticles. Thus, pH is one of the important factors for synthesis of spherical monodisperse nanoparticles [88].

6.2 Morphology of nanoparticles

The size and shape of the synthetized nanoparticles, their total morphology, they were characterized by SEM.

6.2.1 SiO₂ nanoparticles

The size of SiO$_2$ nanoparticles in the samples had various sizes in range 150–750 nm. The size of particles was controlled by different quantities of used chemicals. In the previous research, it was investigated that the diameter of nanoparticles is affected mainly by the concentrations of ammonia and TEOS [89]. Also, an increase of TEOS concentration should increase the polydispersity of synthetized nanoparticles [90]. Hence, these solvents should be crucial in the synthesis of nanoparticles. Another important condition is smoothly stirring of solution during the synthesis. A stirring rate can influence growth, polydispersity and stability of silica nanoparticles [91].

The morphology of nanoparticles was spherical. High monodispersity of the nanoparticles with required size around 290 nm were obtained (*Figure 33*). In the samples was not aggregation.
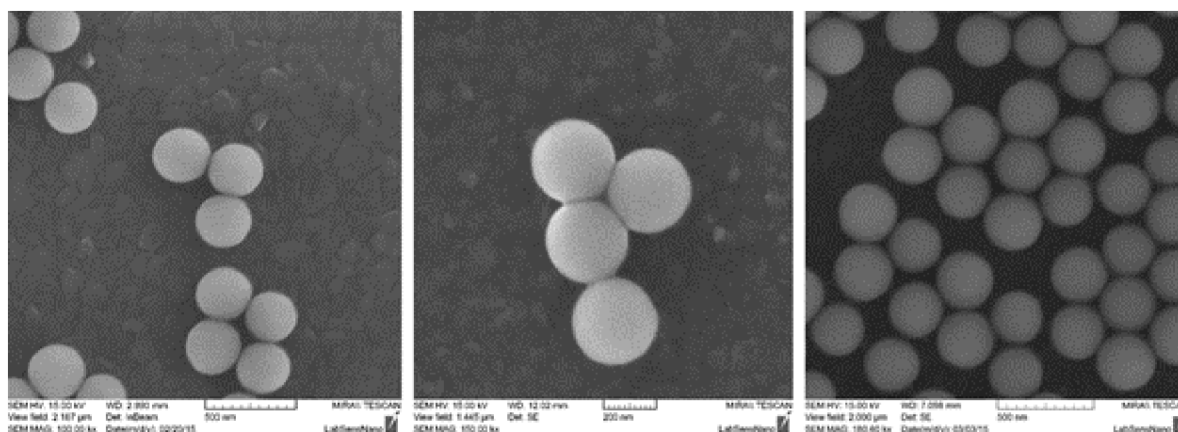
Figure 33: SEM images of the synthetized SiO₂ nanoparticles with the size around 290 nm; sample C1 (left), sample D1 (middle), sample E (right)

Different conditions of synthesis were studied in the process ofSiO$_2$/Au core/shell nanoparticle formation. It was studied an influence of reaction time for the nanoparticle formation. Nanoparticles synthetized with longer times of reactions achieved larger sizes. Also, the formation of particles was more spherical, there were no aggregates. *Figure 34* illustrates the nanoparticles, where synthetized reaction lasted only 2 hours. The size of nanoparticles is only 120 nm and the nanoparticles have nonspherical shape.
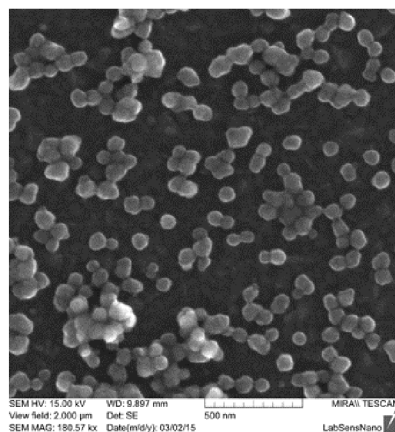
Figure 34: SEM image of SiO$_2$ nanoparticles with 2 hour reaction time (sample X)

Moreover, there were examined the various ratios of reagents in the synthesis. Ammonia in the reaction is used as a catalyst and increases the rate of hydrolysis [85]. The prediction, the higher amount of ammonia in the solution affects to the size of nanoparticles and increases their size, was demonstrated [89]. *Figure 35* illustrates two samples of nanoparticles where sample in the right side contains triple amount of ammonia in comparing with the sample on the left and the nanoparticles have size 500-600 nm. In the first sample nanoparticles have size only about 300 nm.
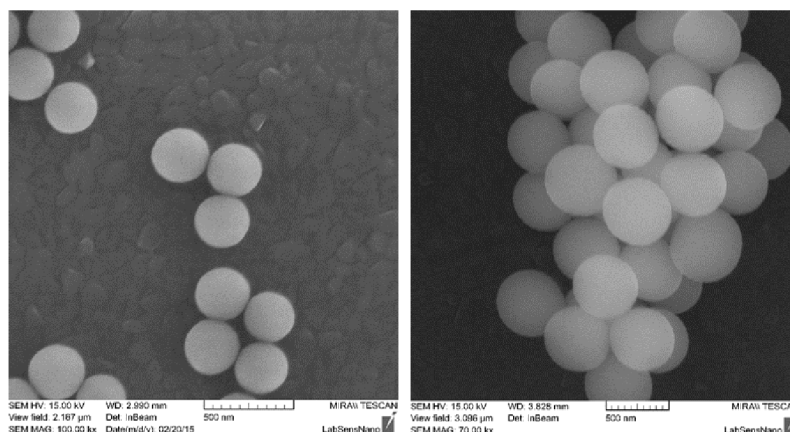
Figure 35: SEM images of synthetizedSiO$_2$nanoparticles with different sizes caused by different concentrations of ammonia; sampleC1 (left), sample B2 (right)

The nanoparticles size should also increase with the increasing concentration of TEOS without significant changes in the size or shape of nanoparticles [92]. The nanoparticles with different concentration of TEOS and the similar quantities of others reagents achieved similar results in the size. However, the polydispersity of the samples could be caused by fast dropping of TEOS into the solution.

The used type of alcohol in reaction plays also important role for the size of nanoparticles in the synthesis. Alcohol serves as a reaction medium. The formation of larger

47

nanoparticles was observed in the sample containing IPA in comparing with EtOH samples. Nanoparticles synthetized with different type of alcohol are illustrated in *Figure 36*. The same ratio of all other reagents was used in both samples. Formation of larger nanoparticles is observed in the sample with IPA where nanoparticles achieved size 550–750 nm. The nanoparticles with EtOH have size around 300 nm.
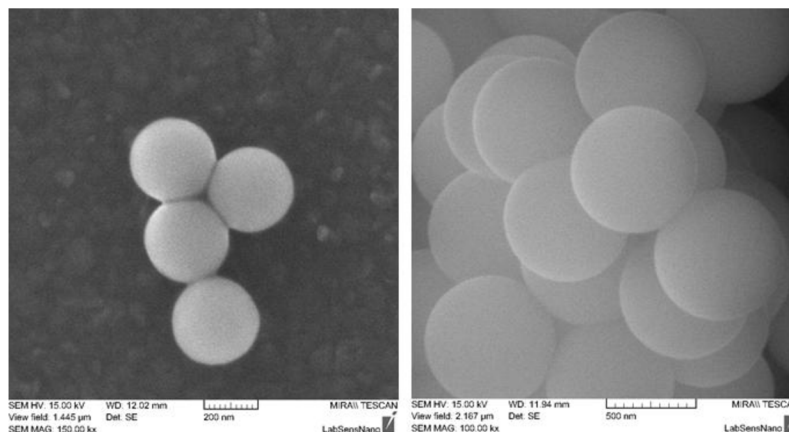
Figure 36: SEM image of SiO₂ nanoparticles with different sizes influenced by type of used alcohol in reaction; sample D1 (left), sample D2 (right)

There was not achieved noticeable different in the formation of nanoparticles synthesized by synchronized hydrolysis. The synchronized hydrolysis was happening between APTES and TEOS. The ratios of used chemicals were used on the base of recipe for formation of 290 nm nanoparticles. There was difference only in the time of adding APTES to the mixtures of solutions. It was obtained that by adding APTES to the solution minimally after 2 hours of reaction, the formation of synthetized nanoparticles was spherical and monodispersed *(Figure 37)*.
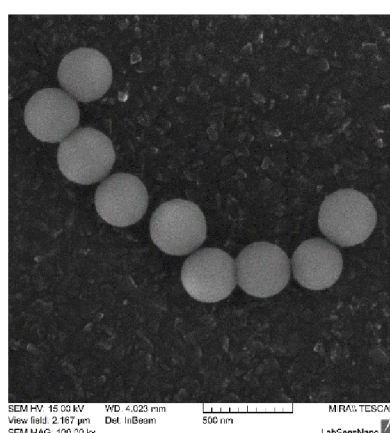
Figure 37: SEM image of SiO₂ nanoparticles synthetized by synchronized hydrolysis (sample Y)

6.2.2 SiO$_2$/Au core/shell nanoparticles

Following figures demonstrate the SEM images of SiO$_2$/Au core/shell nanoparticles. There is illustrated thin shell of attached 1-2 nm gold nanoparticles to the APTES functionalized SiO$_2$ particle cores. The silica cores were coated uniformly in some samples, however only by ultrathin shell of the gold colloids. There were used different concentrations of reagents in synthesis of silica/gold core/shell nanoparticles and also in the growing process of gold nanoshells. Samples which were 2 times functionalized by APTES (Y and Z) not achieved considerable difference in the attachment of gold colloid on the silica surface in comparing with another samples. In the first samples were obtained gold clusters attached on the silica core surface. They contained high quantity of gold colloid and gold plating solution was. This aggregation of gold is illustrated in *Figure 38.*
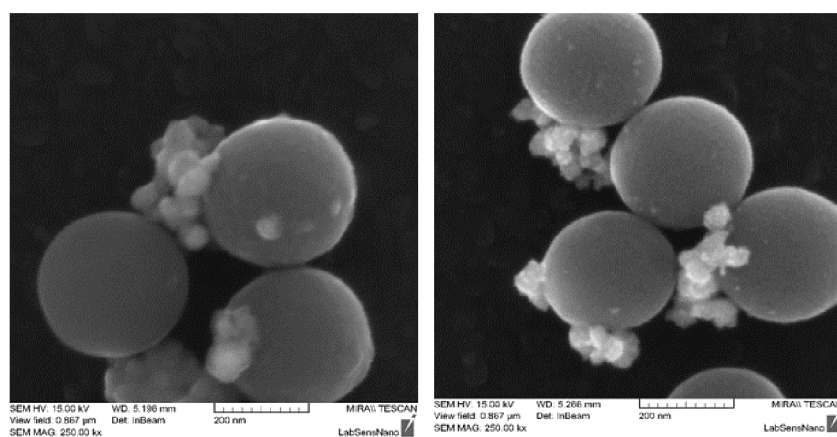
Figure 38: SEM image of synthetized SiO2/Au core shell nanoparticles with aggregation of the gold on the silica surface; sample 1Z (left), sample 1E (right)

It was tested the influence of the aging of gold plating solution for the process of attachment of gold colloidal nanoparticles to the silica surface. Silica nanoparticles were here placed to the fresh gold plating solution. There was obtained only ultrathin layer of the attached gold nanoparticles on the APTES functionalized silica surface. It is shown in the *Figure 39* below.
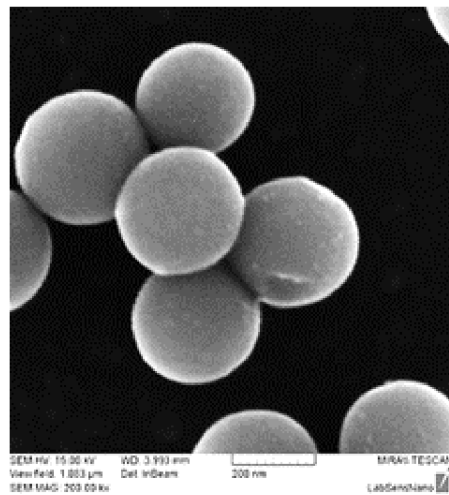
Figure 39: SEM image of synthetized nanoparticles with ultrathin layer of the gold nanoparticles attached on the silica cores (sample 4E)

The higher quality of gold layer was observed by 3 days storing of the gold plating solution, which was used in the process of synthetized SiO_2/Au core/shell nanoparticles. The nanoparticles were coated by thicker and more uniform layer of the gold nanoparticles *(Figure 40)* but the coating by the gold layer is still not adequate. However, it is possible to note that the influence of the age of plating solution for attachment of gold colloidal nanoparticles plays important role in this synthesis.
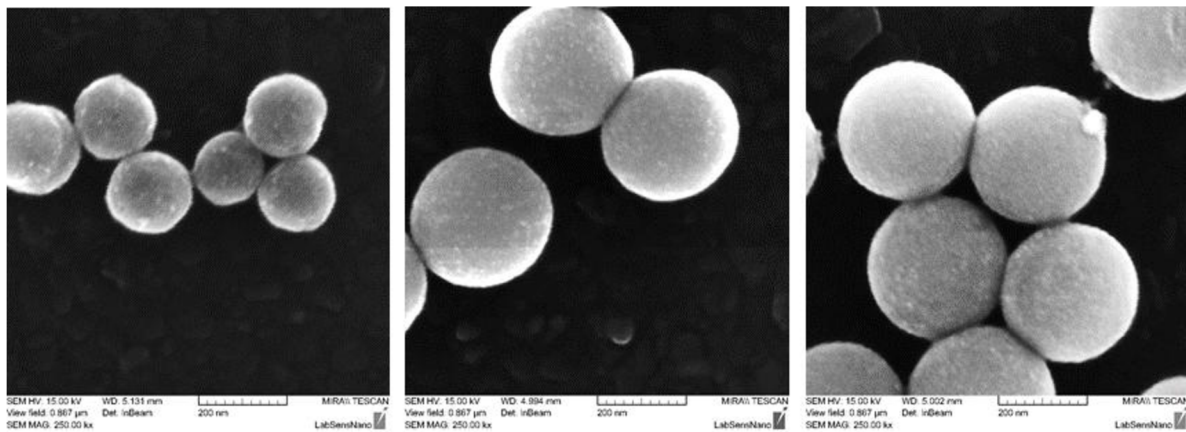
Figure 40: SEM images of synthetized nanoparticles with gold nanoshell on the silica cores; sample 1Y (left), sample 2E (middle), sample 3E (right)

6.3 Size distribution of nanoparticles

Dynamic light scattering (DLS) analysis can determinate more accurately the size and the dispersity of particles in the sample in comparing with SEM. Following graphs illustrate size of nanoparticles which is based on the intensity, volume and number. The intensity distribution illustrates the quantity of scattered light by nanoparticles in different bins. The volume distribution describes the total volume of nanoparticles in the different size bins. The number distribution shows the number of nanoparticles with different size. There are also shown histograms for individual samples.
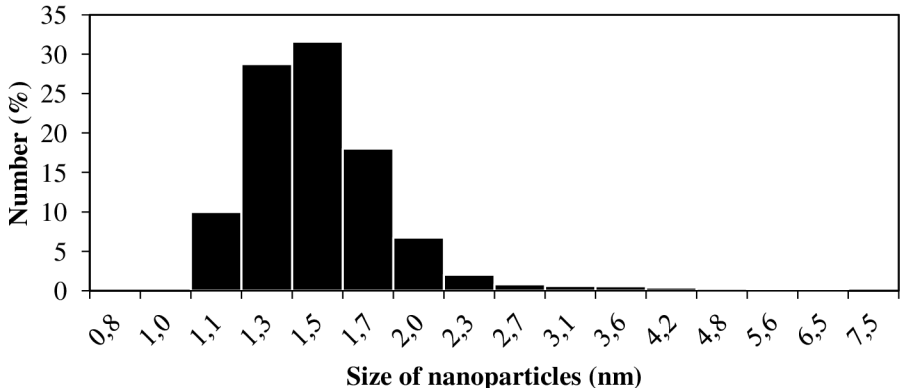
Figure 41: Histogram representing the percentage of individual particle sizes

In the sample of gold colloid fabricated by Duff, 1-3 nm sizes of gold nanoparticles are obtained. These size distribution correspond to the required sizes of nanoparticles. Number distribution shows the majority of recent nanoparticles in the size about 1-2 nm *(Figure 42)*. Nevertheless, the peak of intensity distribution in the area about 100 nm can show the presence of dust.
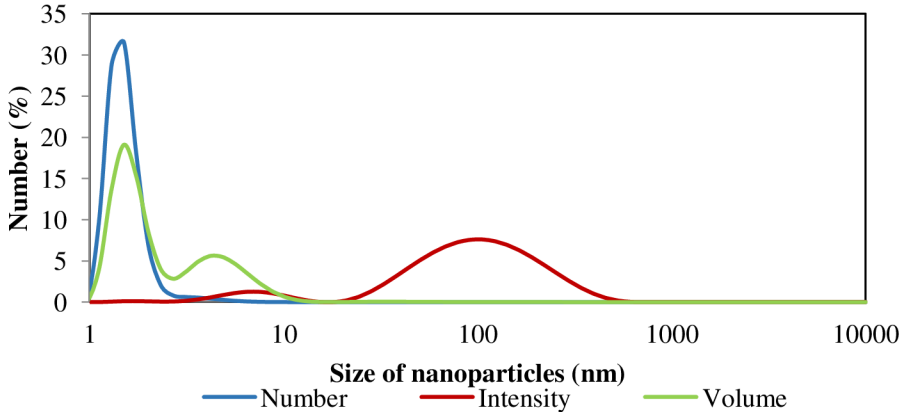
Figure 43: spectrum of DLS analysis with number, size and volume distribution of gold nanoparticles synthetized by Duff

Graf illustrated in *Figure 43,* shows the peaks of intensity, volume and number with narrow spectrum what means, there is narrow distribution size of nanoparticles. These results correspond also with the values obtained from histogram of this sample
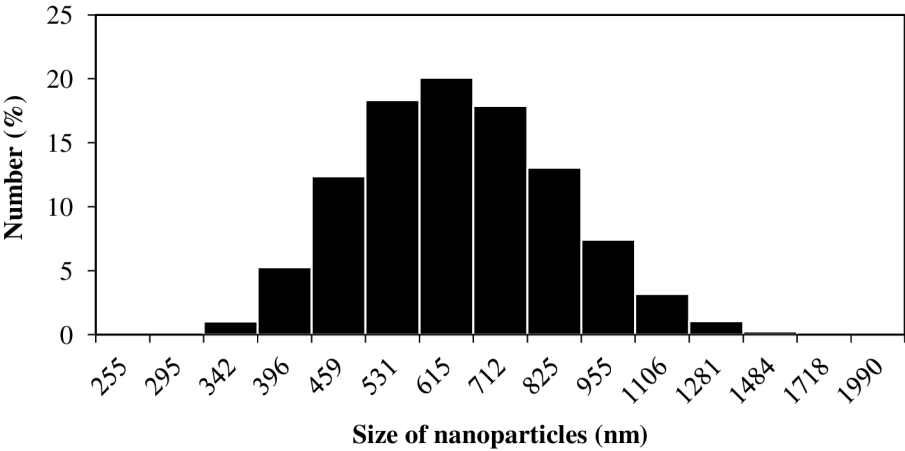
Figure 44: Histogram representing the percentage of individual particle sizes

In the histogram illustrated in *Figure 44* are shown different sizes of nanoparticles. This sample is very polydisperse, nanoparticles have size from 340 nm to 1280 nm. Required size of nanoparticles was 300 nm, which were obtained by SEM. There are possible aggregations of nanoparticles what could be caused by age of sample *(Figure 45)*. On the basis of results from individual distributions, all spectrum are similar and have peak in the same area about 600-700 nmwhat correspond to the results from histogram.
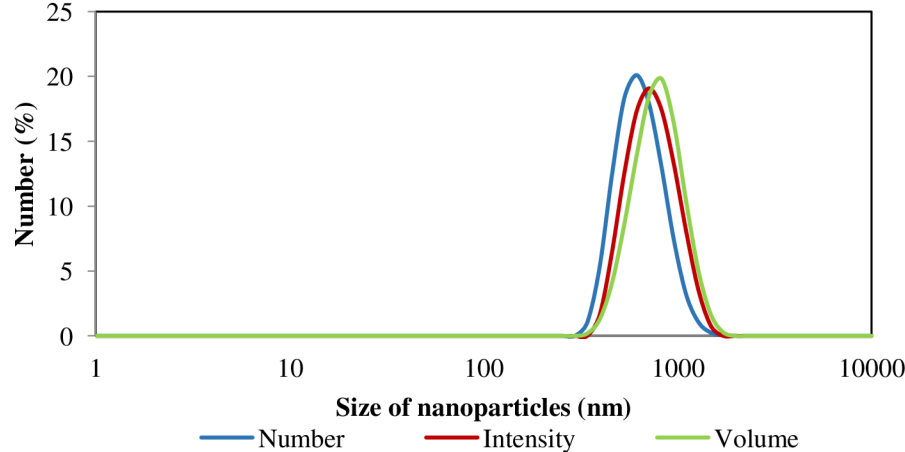
Figure 45: Spectrum of DLS analysis with number, size and volume distribution of SiO$_2$/Au nanoparticles
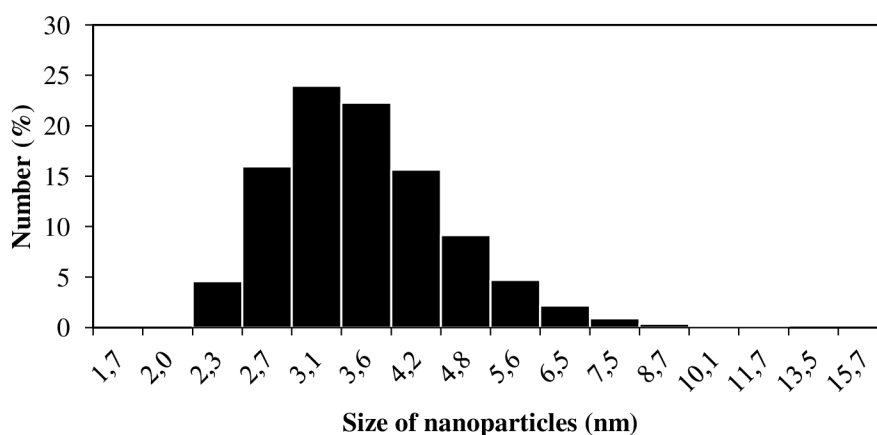
Figure 46: Histogram representing the percentage of individual particle sizes

Expected sizes of commercial nanorods in this sample were around 10 nm. The majority of particles in this sample have around 3 nm size (over 50%) what is obtained from histogram shown in (*Figure 46*). In the histogram and in the spectrum with number, size and intensity distributions, it is possible to see all peaks in the area under 10 nm, in the area aroun 3-4 nm. *(Figure 47*).
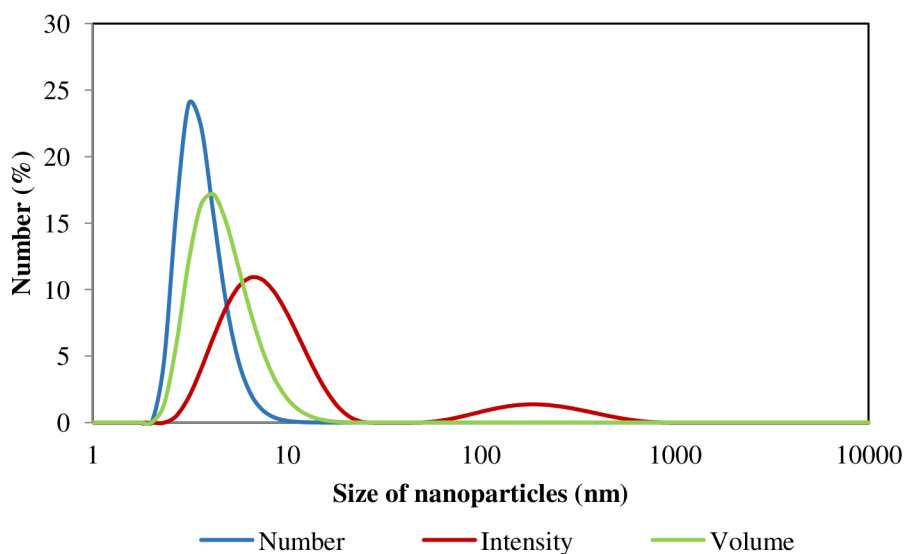
Figure 47: Spectrum of DLS analysis with number, size and volume distribution of gold nanorods with the 10 nm sizes
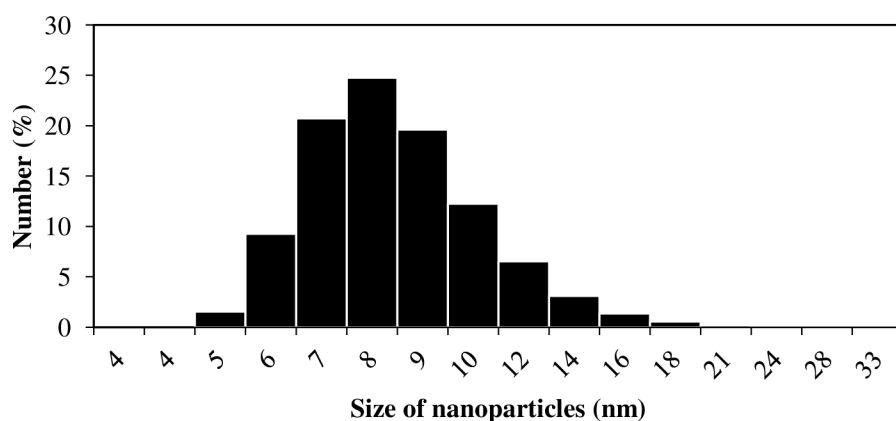
Figure 48: Histogram representing the percentage of individual particle sizes

The commercial nanorods in this sample should have sizes around 25 nm. However the nanorods are again smaller with the size from 5 nm to 18 nm (*Figure 48*). Sample is polydisperse what it is possible to see also from the distribution of intensity in the graph below *(Figure 49).* That shows the intensity of scattered light from the gold nanorods. Number distribution illustrates high amount of nanorods with the size around 8-9 nm, which are the most recent in the histogram above.
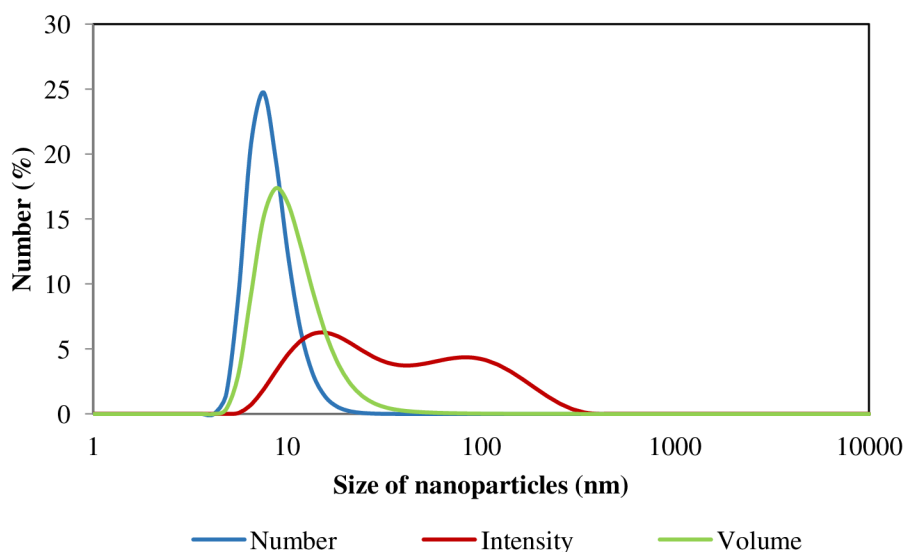
Figure 49: Spectrum of DLS analysis with number, size and volume distribution of gold nanorods with the 25 nm sizes

6.4 Molecular structure of nanoparticles

Another verification of the synthetized nanoparticles structure was performed by FT-IR spectroscopy. The following graph (*Figure 50*) illustrates FT-IR spectrum of SiO_2/Au core/shell synthetized nanoparticles. That was used to identify the complex structure.

All absorption bands should correspond to the concrete frequency for specific functional group. Absorption band in area around 1110 cm^{-1} arises from asymmetric vibration of Si-O, band in area around 945 cm^{-1} arises from asymmetrical vibration of Si-OH and the absorption band in area around 795 cm^{-1} arises from symmetric vibration of Si-O. All these measured values correspond to the values in the FT-IR spectrum of SiO_2/Au nanoparticles which is illustrated in *Figure 23*. Characteristic absorption bands in the area 3300-3500 cm^{-1} determine the O-H band. The peak at 3445 cm^{-1} determinates the NH_2 bond and indicates the presence of the amine groups on the surface of the SiO_2 core nanoparticles. This peak, in the spectrum below is situated in the area around 3380 cm^{-1} indicating that the concentration of amine groups attached on the silica surface is insufficient. Therefore the functionalization of SiO_2 core was possibly nonsatisfied.
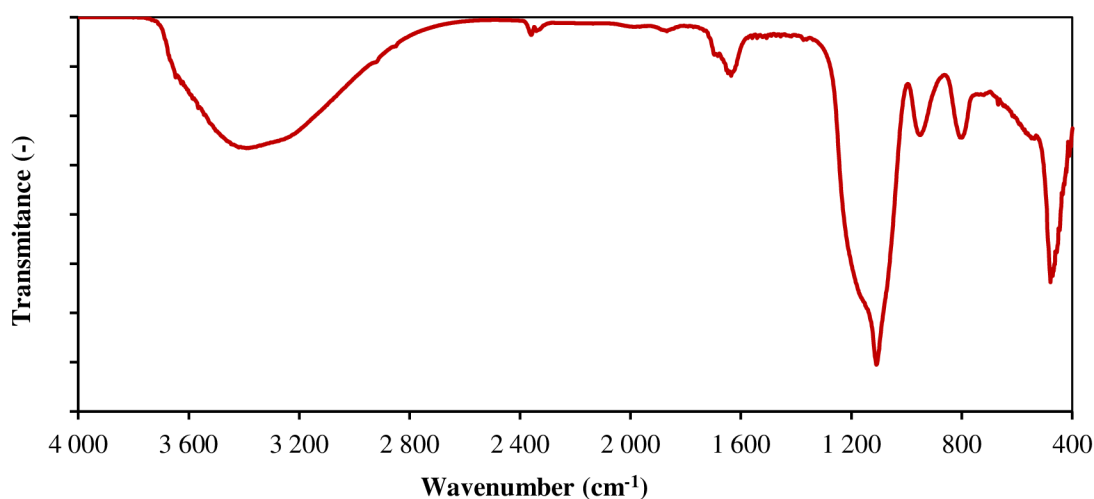
Figure 50: FT-IR spectrum of SiO₂/Au synthetized nanoparticles

6.5 Optical properties of nanoparticles

Nanoparticles have unique optical properties, which are tunable to their size and shape. They offer strong backscattering and absorption. Optical absorption spectra recorded by Uv-Vis spectroscopy and NIR spectroscopy can detect the plasmon resonance peaks in the spectrum of specific molecule.

6.5.1 Absorption spectrum in the visible region

The following graph in *Figure 51* shows the spectra of optical absorption of SiO_2 nanoparticles, bare gold nanoparticles and SiO_2/Au core/shell nanoparticles recorded by UV-Vis spectroscopy.
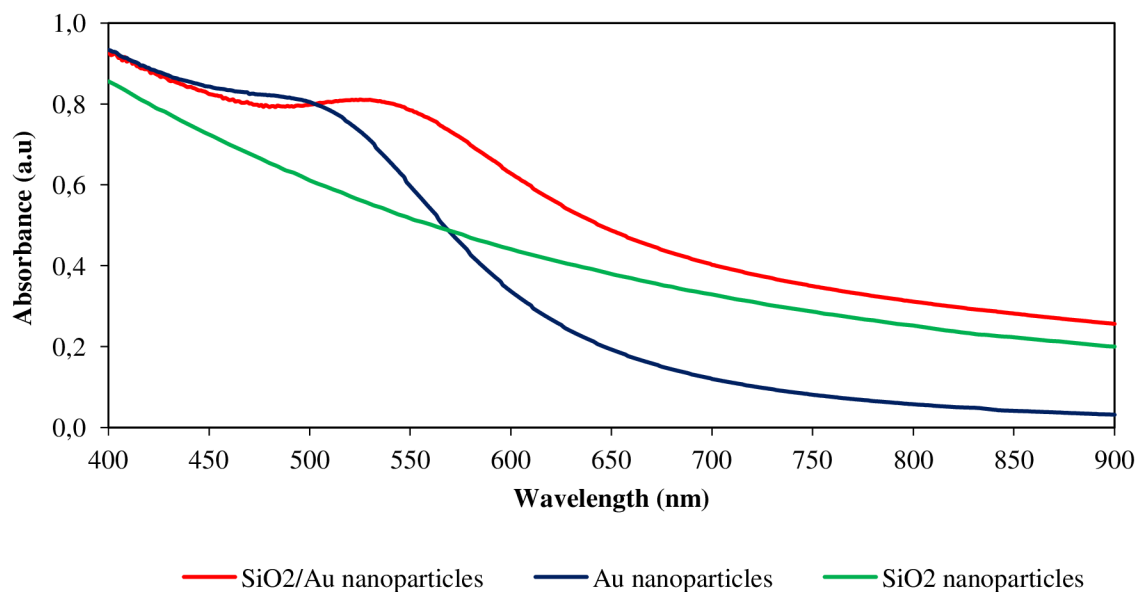
Figure 51: UV-Vis spectrum of silica nanoparticles, gold nanoparticles and SiO₂/Au synthetized nanoparticles

These spectrum with the values of resonance peaks of concrete sample were compared with the spectrum which was illustrated in *Figure 24*. There were examined the same structures of nanoparticles with the same sizes. The resonance plasmon peak of SiO_2/Au nanoparticles in UV-Vis spectrum should be in area around 600 nm for 300 nm size nanoparticles. The intensity of the peak for SiO_2/Au core/shell nanoparticles should spread and decrease, and mainly red shift in comparing with the spectrum of gold nanoparticles. It demonstrates that as more gold chloride is reduced on an attached gold particle, their aspect ratio increases. Absorption peak in the synthetized sample of gold nanoparticles was measured in the area around 490 nm and it shifts only to 525 nm for SiO_2/Au nanoparticles. Although this result not corresponds to the result in graph in *Figure 24*, there is obtained the shift of the SPR peak ofSiO_2/Au nanoparticles towards NIR spectral region. As the NIR shift in spectrum depends on the increasing the core-radius shell thickness ratio, synthetized nanoparticles can have different thickness of the gold shell in comparing with nanoparticles obtained by Nikabaldi *et al.*

In the following graph *(Figure 52)* are shown FT-IR spectrum of synthetized gold nanoparticles prepared by Duff, and spectrum of commercial gold nanorods from Nanopartz with the sizes 10 nm and 25 nm. These samples should have 2 plasmon resonance bands

which are arising from their anisotropic configuration. Those are reflected as 2 distinct peaks in the spectrum. Transverse band corresponds to the oscillation of electrons in the shorter axis and longitudinal band is specific for oscillation in longer axis. This one is very sensitive to changes to the interparticle distance and is depending on the aggregation in the sample [93].
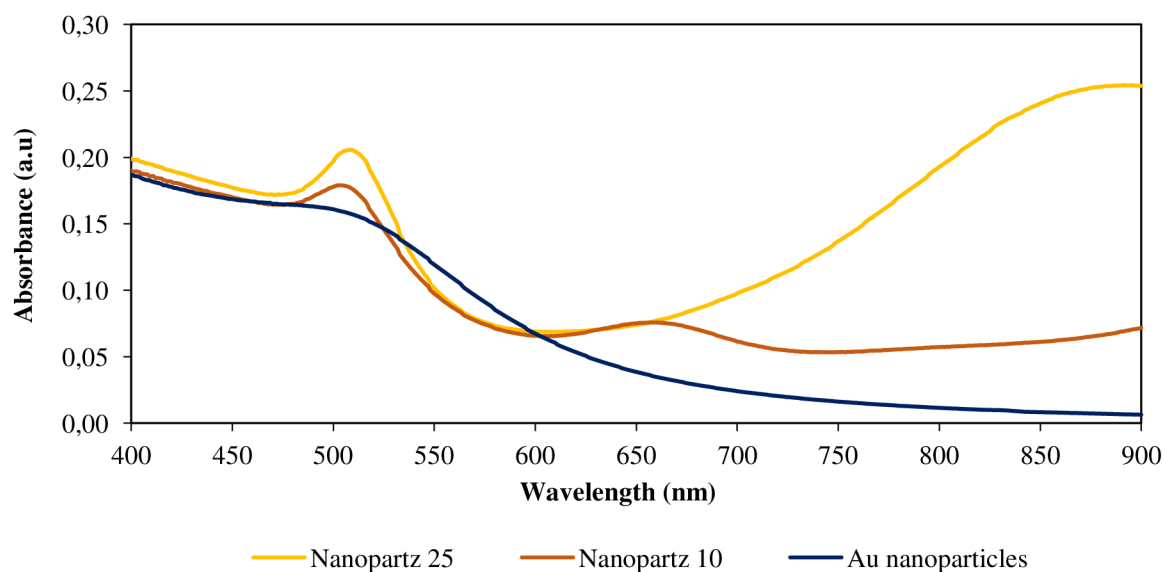
Figure 52: UV-Vis spectrum of synthetized gold nanoparticles and commercial gold nanorods with the size 10 nm and 25 nm

Gold nanoparticles synthetized by Duff have only one plasmon resonance peak in the spectrum at area around 500 nm. Value of peak at this wavelength is also characteristic for both samples of nanorods, what corresponds to the UV-Vis extinction spectrum illustrated in *Figure 22*. The SPR peak of 25 nm nanorods offers stronger absorption at this wavelength in comparing with the sample of 10 nm nanorods (and also in comparing with gold nanoparticles). The second plasmon resonance peak of this sample is situated in NIR region of the spectrum. The sample with the 10 nm size nanorods has second peak at wavelength 659 nm and possibly another appearing peak in longer wavelength in NIR spectrum.

6.5.2 Absorption spectrum in the near-infrared region

NIR spectrum is similar to UV-Vis spectrum only it is located in longer wavelengths. Graphs in *Figure 53* and *Figure 54* show the absorption spectrum for gold nanorods with the size 10 nm. It is possible to see that this type of nanorods is active in the NIR region of the spectrum. The influence of the age of gold nanorods for the shift of SPR peak in the absorption spectrum was examined. The first tested nanorods were examined immediately after delivering and the second sample was stored for 6 months before testing.
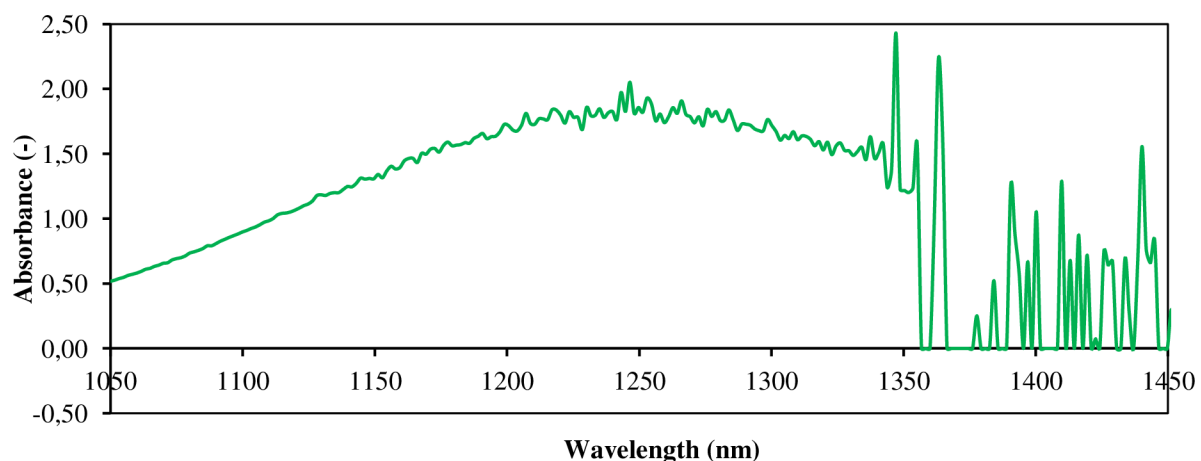
Figure 53: NIR spectrum of the fresh (after delivering) commercial nanorods with the size 10 nm
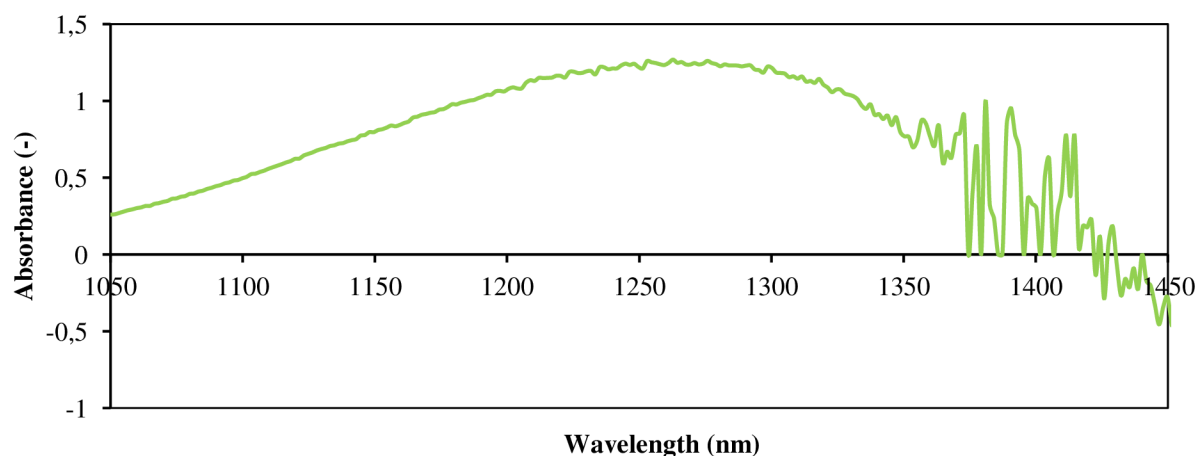
Figure 54: NIR spectrum of the commercial nanorods with the size 10 nm after the 6 months of their storing

In the first sample was recorded stronger absorption spectrum. It means that with aging of nanorods, their optical properties get worse. There was observed no big difference in the location of plasmon resonance peak in the samples. In both samples, it was situated in the area around 1250–1300 nm. Although, the peak in the NIR spectrum of the aged nanorods was shifted approximately about 50 nm toward a longer wavelength in comparing with the fresh nanorods.

6.6 Enhancement of OCT contrast

It was studied the effect of nanoparticles with 200 nm silica cores and 20 nm cold shell diameter on signal enhancement of spectral-domain OCT system CALLISTO. The plasmon resonance of nanoparticles is at 980 nm what corresponds to the OCT system used in this study (central wavelength at 930 nm).

In this study, the nanoparticles were dispersed in Millipore water. The effect of nanoparticles concentration on OCT signal intensity was examined. Different concentrations of nanoparticles were tested: 0.5 mg/mL, 0.25 mg/mL, 0.125mg/mL, 0.062 mg/mL and 0.031 mg/mL (*Figure 55*). In the measurement, the nanoparticles were settling after time. Thus, to get a homogenous suspension of nanoparticles, every suspension was agitated just before the OCT acquisitions.
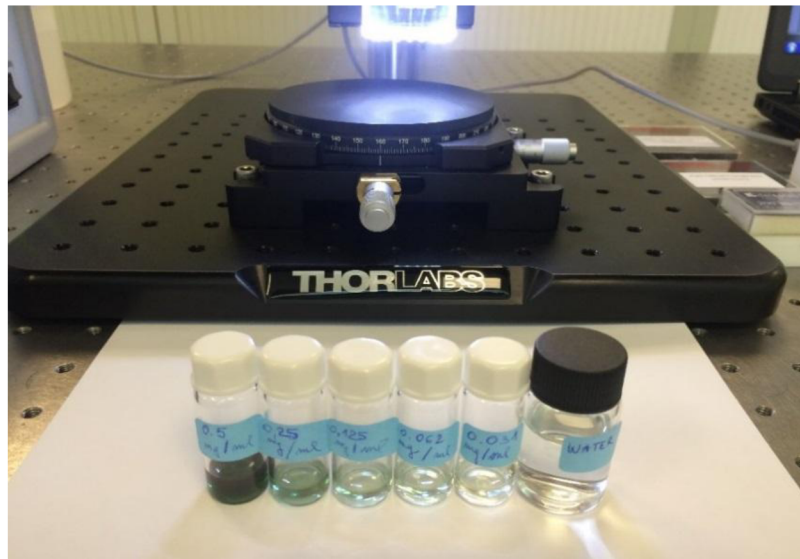
Figure 55: Suspensions of nanoparticles with different concentrations

Figure 55 illustrates the B-scans of OCT images of water and water containing different concentrations of nanoparticles. The first B-scan corresponds to Millipore water (18.2 MΩcm). It has bad contrast because of low intensity of the scattered light in water. The picture is almost all black. It is possible to see only white line corresponding to the water surface. The contrast of the B-scan in the middle picture is notably improved after adding nanoparticles (0.062 mg/mL) but there is still low enhancement of contrast intensity in the image. With the increasing concentrations of nanoparticles, it increased the intensity of the scattered light what improved the contrast. Last measurement in this study was tested with the concentration 0.5 mg/mL, what is illustrated in the last B-scan in that figure. There was not big different in the enhancement of signal in the measurement with the concentrations of nanoparticles between 0.062–0.5 mg/mL.
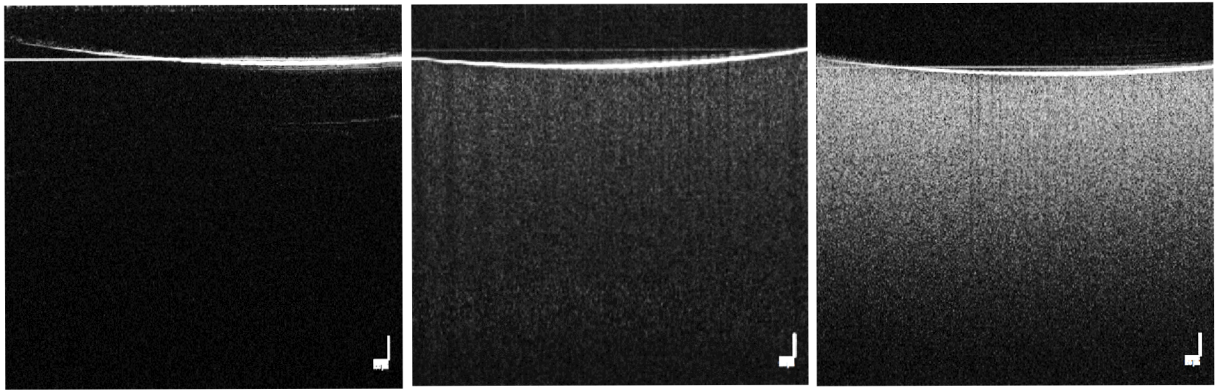
Figure 56: B-scans of OCT images for Millipore water (left); water with nanoparticles (0.062 mg/mL) (middle); water with nanoparticles (0.5 mg/mL) (right)

There were obtained A-scans of Millipore water and water containing nanoparticles with the concentration 0.5 mg/mL. These depth profiles were compared in one graph illustrated below (*Figure 57*). The sample with pure water has base-line in the area around 15 dB. There is achieved an intensity grow to area 30-40 dB in the A-scan of sample containing SiO_2/Au nanoparticles.
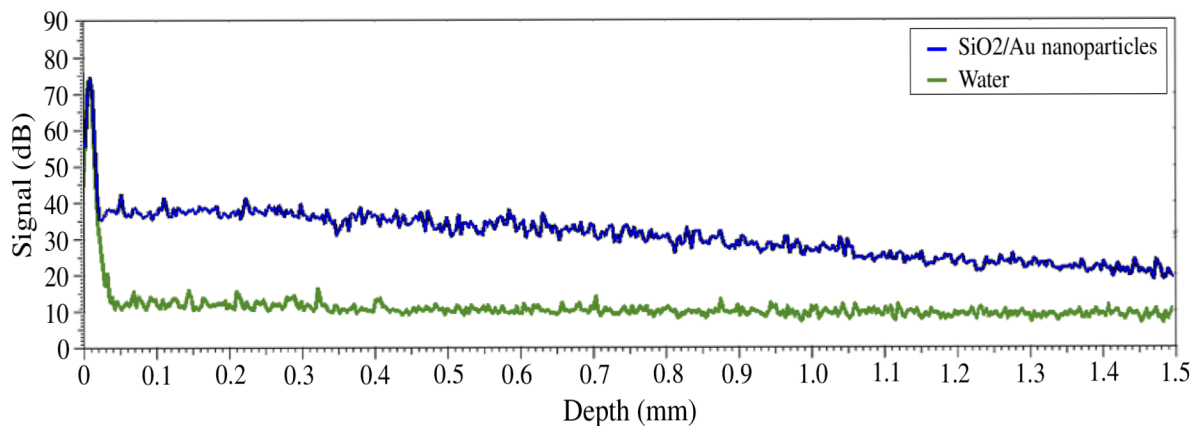
Figure 57: A scans of water and SiO_2/Au nanoparticles with the 0.5 mg/mL concentration dispersed in water

A white line in the B-scans of water and water with nanoparticles, illustrated in *Figure 58*, were used as reference for calculations of the A-scan profiles. These were collected in the depth direction.
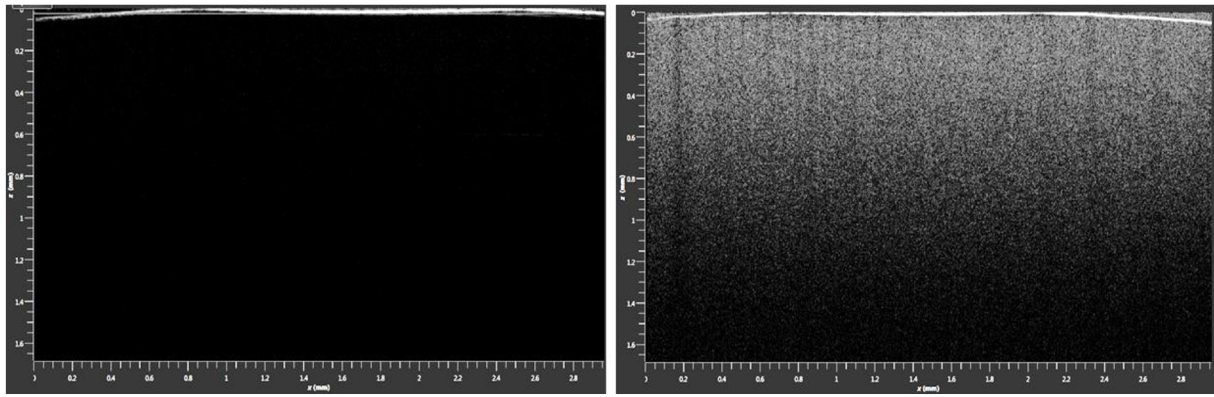
Figure 58: Reference B-scans of Millipore water (left), water with 0.5 mg/mL concentration of nanoparticles (right)

Synthetized SiO_2/Au core/shell nanoparticles were examined for enhancement of optical coherence tomography signal. In this measurement was used the OCT system OCS1300SS. Created signal from the sample containing nanoparticles was compared with a signal from Millipore water. In the OCT image, there was observed evident enhancement of the contrast in the sample with nanoparticles, which is illustrated in *Figure 59*. However, on the base of previous testing (UV-Vis, FR-IR, *etc.*), the results from synthetized nanoparticles not correspond to the required results. Hence, this examination is not objective for the evaluation of contrast enhancement by this type of nanoparticles with this structure.
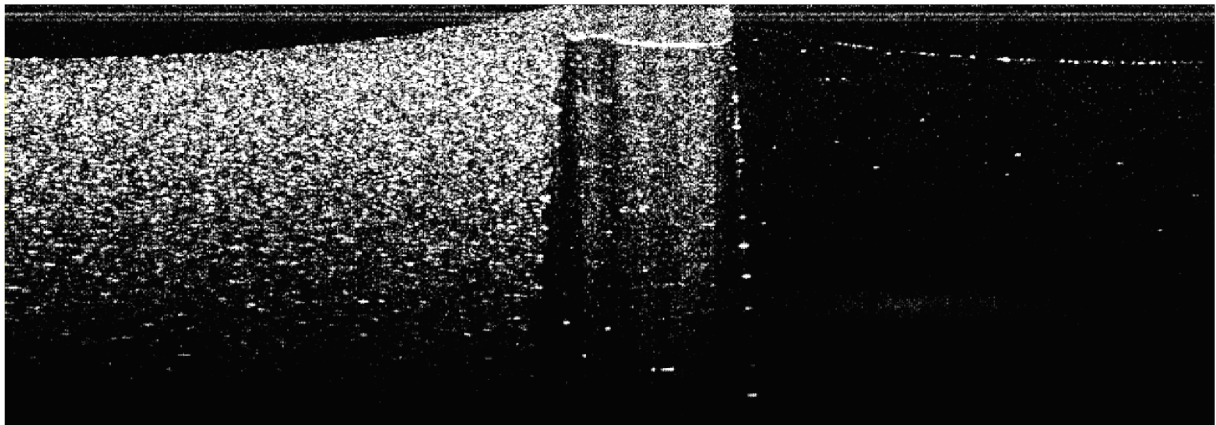
Figure 59: Enhancement of contrast in OCT image by synthetized SiO_2/Au core/shell nanoparticles (left), by Millipore water (right)

In the following measurements was also employed the OCT system OCS1300SS. The operating wavelength of this system corresponded to the wavelengths of plasmon resonance peaks of the commercial nanorords used in these measurements. Therefore, the OCT signal should achieved the best results in the process of contrast enhancement by this type of nanorods. The same principle of testing was carried out as in the previous case with

synthetized nanoparticles; the obtained signal was compared with the signal from Millipore water.
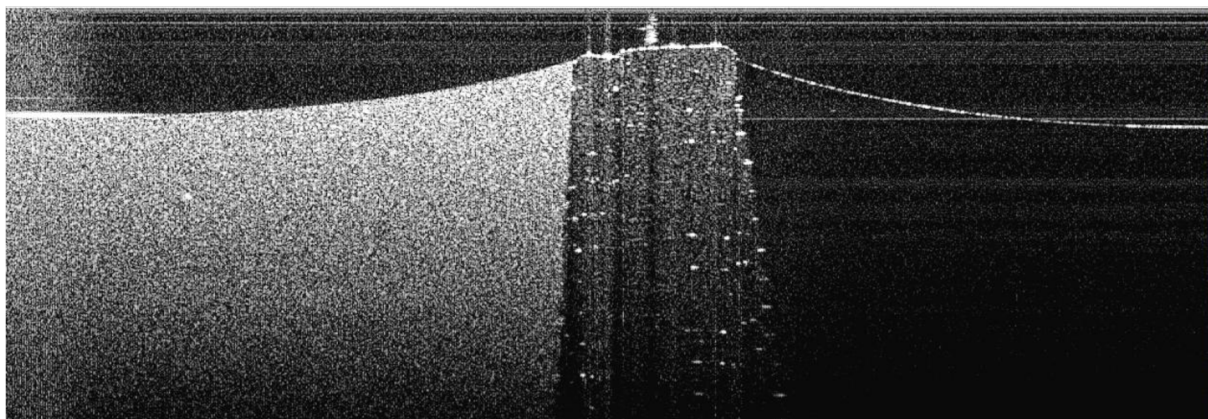
Figure 60: Enhancement of contrast in OCT image by commercial nanorods with the size 25 nm (left), by Millipore water (right)

Both commercial samples with different sizes of nanorods were verified. Better contrast was observed in the first OCT image, where were tested the nanorods with size 25 nm. This effect is illustrated in *Figure 60.* Nanorods with the 10 nm size did not improve the OCT contrast so strongly *(Figure 61)*.
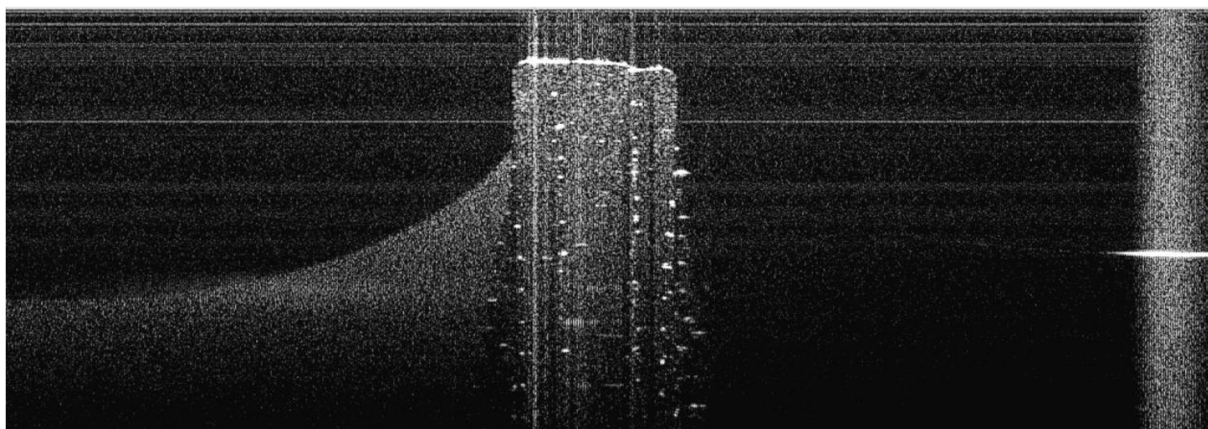
Figure 61: Enhancement of contrast in OCT image by commercial nanorods with the size 10 nm (left), by Millipore water (right)

Although the silica/gold core/shell nanoparticles were not synthetized with enough thick layer of gold, they achieved the greatest contrast of OCT image from all 3 samples in this measurement. Even if the nanoparticles had the SPR peak in the area around 525 nm and central wavelength of OCT was at 1300 nm.

7 Conclusion

This work was aimed at synthesis of nanoparticles, with 290 nm size of silica core coated by thin layer of gold, which should improve the intensity of optical coherence tomography signal. For the synthesis of silica nanoparticles was used Stöber method. Synthetized nanoparticles were subsequently functionalized by APTES and covered by gold colloid which was fabricated by the process of Duff.

After synthesis, chemical, physical and optical properties of synthetized nanoparticles were tested using a variety of techniques. The resulting size, shape and total morphology of nanoparticles were examined by SEM. Final particles were monodispersed with the required final size around 300 nm. Size distribution of the nanoparticles in the sample was obtained by DLS. This technique was used for examination of commercial gold nanorods purchased from Nanopartz. UV-Vis spectroscopy and NIR spectroscopy were used to determinate the surface plasmon resonance peaks of specific molecules in the spectrum. These values of wavelengths, in which occur to the enhancement of the light intensity should be for synthetized SiO_2/Au particles with the size 300 nm, in wavelength about 600 nm [13]. However synthetized nanoparticles had this peak in the wavelength around 530 nm. Absorption peaks in spectrum of commercial nanoparticles from NIR spectroscopy corresponded to the required values. Then, chemical composition of silica/gold nanoparticles was determined by FT-IR spectroscopy. Synthetized nanoparticles did not contain sufficient concentrations of amine groups in the corresponding band. Thus, the silica surface was covered by gold nanoparticles only in ultrathin shell. Therefore, functionalization by APTES requires optimization to create suitable nucleation sites on the silica surface for the better attachment of gold colloid.

In the last step, the synthetized SiO_2/Au nanoparticles were tested for enhancement of OCT signal as contrast agents. For this testing were also used commercial silica/gold nanoparticles from NanoComposix and also gold nanorods. Two different OCT system were used for this examination, OCT system CALLISTO and system OCT system OCS1300SS, both from Thoralbs. In all samples was observed enhancement of the OCT signal. Commercial silica/gold core/shell nanoparticle were testing for enhancement of signal in different concentrations. It was observed that with the higher concentrations of particles, the OCT contrast in image was improved. The best results were achieved in the synthetized SiO_2/Au core/shell nanoparticles, however the structure of these nanoparticles did not achieved required properties. It is necessary to optimalizate the functionalization of silica cores of these nanoparticles and ensure more uniform attachment of gold colloid.

List of abbreviations

1D – 1 dimensional

2D – 2 dimensional

3D – 3 dimensional

APTES – 3-Aminopropyltriethoxysilane

BSE – backscattered electrons

CAS No – chemical abstracts service number

CT – computed tomography

DI – distilled water

DLS – dynamic light scattering

EBSD – diffracted backscattered electrons

EDX – energy dispersive X-ray

FT-IR– Fourier transform-infrared spectroscopy

IPA – isopropyl alcohol

IR – infrared radiation

LED–light-emitting diode

MRI –magnetic resonance imaging

NIR – near infrared radiation

NIRS – near infrared spectroscopy

OCT – optical coherence tomography

PEG – polyethylene glycol

PET – positron emission tomography

PS – plating solution

SD-OCT – spectral domain optical coherence tomography

SEM – scanning electron microscopy

SPR – surface plasmon resonance

TD-OCT – time domain optical coherence tomography

TEM – transmission electron microscopy

TEOS – tetraethoxysilane

THPC – hydroxymethyl-phosphonium chloride

TMOS – tetramethosxysilane

US – ultrasound

UV-Vis – ultraviolet-visible spectroscopy

Bibliography

[1]   LOGOTHETIDIS, S. Nanotechnology in medicine: the medicine of tomorrow and nanomedicine. *Hippokratia*, 2006, vol. 10, no. 1, pp. 7-21. ISSN 1790-8019.

[2]   JAIN, S. et al. Gold nanoparticles as novel agents for cancer therapy. *The British journal of radiology*, 2012, vol. 85, no. 1010, pp. 101-113.

[3]   HAHN, M. et al. Nanoparticles as contrast agents for in-vivo bioimaging: current status and future perspectives. *Analytical and Bioanalytical Chemistry*, 2011, vol. 399, no. 1, pp. 3-27. ISSN 1618-2642.

[4]   SLOWING, I. I. et al. Mesoporous silica nanoparticles as controlled release drug delivery and gene transfection carriers. *Advanced Drug Delivery Reviews*, 2008, vol. 60, no. 11, pp. 1278-1288. ISSN 0169-409X.

[5]   GELPERINA, S. et al. The Potential Advantages of Nanoparticle Drug Delivery Systems in Chemotherapy of Tuberculosis. *American Journal of Respiratory and Critical Care Medicine*, 2005, vol. 172, no. 12, pp. 1487-1490. ISSN 1073-449X.

[6]   NAZARENUS, M. et al. In vitro interaction of colloidal nanoparticles with mammalian cells: What have we learned thus far? *Beilstein Journal of Nanotechnology*, 2014, vol. 5, pp. 1477-1490. ISSN 2190-4286.

[7]   BERRET, J.-F. et al. Controlled clustering of superparamagnetic nanoparticles using block copolymers: design of new contrast agents for magnetic resonance imaging. *Journal of the American Chemical Society*, 2006, vol. 128, no. 5, pp. 1755-1761. ISSN 0002-7863.

[8]   WANG, Y. et al. Mesoporous silica nanoparticles in drug delivery and biomedical applications. *Nanomedicine: Nanotechnology, Biology and Medicine*, 2015, vol. 11, no. 2, pp. 313-327. ISSN 1549-9634.

[9]   BITAR, A. et al. Silica-based nanoparticles for biomedical applications. *Drug Discovery Today*, 2012, vol. 17, no. 19–20, pp. 1147-1154. ISSN 1359-6446.

[10]   ROSENHOLM, J. M. et al. Towards multifunctional, targeted drug delivery systems using mesoporous silica nanoparticles - opportunities & challenges. *Nanoscale*, 2010, vol. 2, no. 10, pp. 1870-1883. ISSN 2040-3364.

[11]   RAHMAN, I. A. et al. Size-dependent physicochemical and optical properties of silica nanoparticles. *Materials Chemistry and Physics*, 2009, vol. 114, no. 1, pp. 328-332. ISSN 0254-0584.

[12]   YUFANG, Z. Functional Mesoporous Silica Nanoparticles with a Core-Shell Structure for Controllable Drug Delivery. In *Advanced Bioactive Inorganic Materials for Bone Regeneration and Drug Delivery.* CRC Press, 2013, pp. 47-82.

[13]   AGRAWAL, A. et al. Quantitative evaluation of optical coherence tomography signal enhancement with gold nanoshells. *Journal of biomedical optics*, 2006, vol. 11, no. 4, pp. 041121-041121-041128. ISSN 1083-3668.

[14]   HU, Y. et al. Optical properties of gold-silica-gold multilayer nanoshells. *Optics Express*, 2008, vol. 16, no. 24, pp. 19579-19591.

[15]   LIU, S. a HAN, M.-Y. Silica-Coated Metal Nanoparticles. *Chemistry – An Asian Journal*, 2010, vol. 5, no. 1, pp. 36-45. ISSN 1861-471X.

[16]   EDMUNDSON, M. C. et al. Exploring the potential of metallic nanoparticles within synthetic biology. *New Biotechnology*, 2014, vol. 31, no. 6, pp. 572-578. ISSN 1871-6784.

[17]   RAVISHANKAR RAI, V. a JAMUNA BAI, A. Nanoparticles and their potential application as antimicrobials. *Science against microbial pathogens: communicating current research and technological advances. FORMATEX*, 2011, pp. 197-209.

[18]   DYKMAN, L. a KHLEBTSOV, N. Gold nanoparticles in biomedical applications: recent advances and perspectives. *Chemical Society Reviews*, 2012, vol. 41, no. 6, pp. 2256-2282. ISSN 0306-0012.

[19]   WANI, I. A. a AHMAD, T. Size and shape dependant antifungal activity of gold nanoparticles: A case study of Candida. *Colloids and Surfaces B: Biointerfaces*, 2013, vol. 101, no. 0, pp. 162-170. ISSN 0927-7765.

[20]   KRPETIĆ, Ž. Centre for BioNano Interactions launches , FutureNanoNeeds Project 2014.

[21]   AHN, S. et al. Gold nanoparticle contrast agents in advanced X-ray imaging technologies. *Molecules*, 2013, vol. 18, no. 5, pp. 5858-5890.

[22]   TUERSUN, P. a HAN, X. E. Optimal dimensions of gold nanoshells for light backscattering and absorption based applications. *Journal of Quantitative Spectroscopy and Radiative Transfer*, 2014, vol. 146, pp. 468-474. ISSN 0022-4073.

[23]   KELLY, K. L. et al. The optical properties of metal nanoparticles: the influence of size, shape, and dielectric environment. *The Journal of Physical Chemistry B*, 2003, vol. 107, no. 3, pp. 668-677. ISSN 1520-6106.

[24]   HUANG, X. a EL-SAYED, M. A. Gold nanoparticles: optical properties and implementations in cancer diagnosis and photothermal therapy. *Journal of Advanced Research*, 2010, vol. 1, no. 1, pp. 13-28. ISSN 2090-1232.

[25]   MIE, G. Contributions to the optics of turbid media, particularly of colloidal metal solutions. *Contributions to the optics of turbid media, particularly of colloidal metal solutions Transl. into ENGLISH from Ann. Phys.(Leipzig), v. 25, no. 3, 1908 p 377-445*, 1976, vol. 1, pp. 377-445.

[26]   SIGMA-ALDRICH. Gold Nanoparticles: Properties and Applications. [online]. [cit. 30.06. 2015]. Available from: <http://www.sigmaaldrich.com/materials-science/nanomaterials/gold-nanoparticles.html>.

[27]   JAIN, P. K. et al. Calculated absorption and scattering properties of gold nanoparticles of different size, shape, and composition: applications in biological imaging and biomedicine. *The Journal of Physical Chemistry B*, 2006, vol. 110, no. 14, pp. 7238-7248. ISSN 1520-6106.

[28]   SURESH, S. Semiconductor Nanomaterials, Methods and Applications: A Review. *Nanoscience and Nanotechnology*, 2013, vol. 3, no. 3, pp. 62-74. ISSN 2163-2588.

[29]   SINGH, L. P. et al. Sol-Gel processing of silica nanoparticles and their applications. *Advances in Colloid and Interface Science*, 2014, vol. 214, no. 0, pp. 17-37. ISSN 0001-8686.

[30]   CUNNINGHAM, A. a BÜRGI, T. Bottom-up Organisation of Metallic Nanoparticles. In ROCKSTUHL, C. a SCHARF, T. *Amorphous Nanophotonics.* Springer Berlin Heidelberg, 2013, pp. 1-37.

[31]   TAVAKOLI, A. et al. A review of methods for synthesis of nanostructured metals with emphasis on iron compounds. *Chemical Papers*, 2007, vol. 61, no. 3, pp. 151-170. ISSN 0366-6352.

[32]   RAO, K. S. et al. A novel method for synthesis of silica nanoparticles. *Journal of Colloid and Interface Science*, 2005, vol. 289, no. 1, pp. 125-131. ISSN 0021-9797.

[33]   ZAINALA, N. A. et al. Study on the Effect of Synthesis Parameters of Silica Nanoparticles Entrapped with Rifampicin. *CHEMICAL ENGINEERING*, 2013, vol. 32.

[34]   WU, S.-H. et al. Synthesis of mesoporous silica nanoparticles. *Chemical Society Reviews*, 2013, vol. 42, no. 9, pp. 3862-3875. ISSN 0306-0012.

[35]   RAHMAN, I. A. a PADAVETTAN, V. Synthesis of silica nanoparticles by sol-gel: size-dependent properties, surface modification, and applications in silica-polymer

nanocomposites—a review. *Journal of Nanomaterials*, 2012, vol. 2012, pp. 8. ISSN 1687-4110.

[36]   JANG, S. et al. Preparation and characterization of conductive polyaniline/silica hybrid composites prepared by sol–gel process. *Synthetic Metals*, 2000, vol. 110, no. 1, pp. 17-23. ISSN 0379-6779.

[37]   GUO, J. et al. Size-controllable synthesis of monodispersed colloidal silica nanoparticles via hydrolysis of elemental silicon. *Journal of Colloid and Interface Science*, 2008, vol. 326, no. 1, pp. 138-142. ISSN 0021-9797.

[38]   HARTLEN, K. D. et al. Facile Preparation of Highly Monodisperse Small Silica Spheres (15 to >200 nm) Suitable for Colloidal Templating and Formation of Ordered Arrays. *Langmuir*, 2008, vol. 24, no. 5, pp. 1714-1720. ISSN 0743-7463.

[39]   Conference ProceedingsLONG, N. N. et al. *Synthesis and optical properties of colloidal gold nanoparticles*. Journal of Physics: Conference Series. IOP Publishing, 1742-6596.

[40]   NAGARAJAN, R. Nanoparticles: building blocks for nanotechnology. *Nanoparticles: Synthesis, Stabilization, Passivation, and Functionalization*, 2008, vol. 996, pp. 2-14.

[41]   AHMAD, T. Reviewing the Tannic Acid Mediated Synthesis of Metal Nanoparticles. *Journal of Nanotechnology*, 2014, vol. 2014, pp. 11.

[42]   OBLIOSCA, J. M. et al. Morphogenesis of anisotropic gold nanostructures stabilized by the greener ionic liquid 1-butyl-3-methylimidazolium lauryl sulfate.

[43]   HANŽIĆ, N. et al. The synthesis of gold nanoparticles by a citrate-radiolytical method. *Radiation Physics and Chemistry*, 2015, vol. 106, pp. 77-82. ISSN 0969-806X.

[44]   BRITO-SILVA, A. M. et al. Improved Synthesis of Gold and Silver Nanoshells. *Langmuir*, 2013, vol. 29, no. 13, pp. 4366-4372. ISSN 0743-7463.

[45]   ANDREW, J. C. a JENNIFER, L. W. Targeting Gold Nanoparticles for Cancer Diagnostics and Therapeutics. In *Functional Nanoparticles for Bioanalysis, Nanomedicine, and Bioelectronic Devices Volume 2*. American Chemical Society, 2012, vol. 1113, pp. 37-54.

[46]   DUFF, D. G. et al. A new hydrosol of gold clusters. 1. Formation and particle size variation. *Langmuir*, 1993, vol. 9, no. 9, pp. 2301-2309. ISSN 0743-7463.

[47]   LANGE, A. P. et al. Time-domain and spectral-domain optical coherence tomography of retinal nerve fiber layer in MS patients and healthy controls. *Journal of ophthalmology*, 2012, vol. 2012. ISSN 2090-004X.

[48]   FUJIMOTO, J. G. et al. Optical coherence tomography: an emerging technology for biomedical imaging and optical biopsy. *Neoplasia*, 2000, vol. 2, no. 1, pp. 9-25. ISSN 1476-5586.

[49]   GOBIN, A. M. et al. Near-infrared resonant nanoshells for combined optical imaging and photothermal cancer therapy. *Nano letters*, 2007, vol. 7, no. 7, pp. 1929-1934. ISSN 1530-6984.

[50]   OPTICIANS, S. B. OCT - (Optical Coherence Tomography). [online]. [cit. 7.7. 2015]. Available from: <http://www.beswetherick-opticians.co.uk/oct/>.

[51]   HOU, R. et al. Recent advances in optical coherence tomography for the diagnoses of lung disorders 2011. ISSN 1747-6348.

[52]   WIJEISNGHE, R. E. H. et al. Wavelength-Filter Based Spectral Calibrated Wave number-Linearization in 1.3 mm Spectral Domain Optical Coherence. *International journal of engineering and advanced technology*, 2013, vol. 3, no. 2, pp. 336.

[53]   FORTE, R. et al. Comparison of time domain Stratus OCT and spectral domain SLO/OCT for assessment of macular thickness and volume. *Eye*, 2009, vol. 23, no. 11, pp. 2071-2078. ISSN 0950-222X.

[54] BRUNO, L. a MARCO, R. *Guide to interpreting spectral domain optical coherence tomography*. JAYPEE BROTHERS PUBLISHERS, 2011. pp. ISBN 9350253844.

[55] YOLCU, U. et al. Imaging in Ophthalmology 2014.

[56] CASTRO LIMA, V. et al. Simultaneous confocal scanning laser ophthalmoscopy combined with high-resolution spectral-domain optical coherence tomography: a review. *Journal of ophthalmology*, 2011, vol. 2011. ISSN 2090-004X.

[57] THORLABS CALLISTO, Spectral Domain OCT System, Operating Manual 2011, pp. 60.

[58] XU, C. et al. Near-infrared dyes as contrast-enhancing agents for spectroscopic optical coherence tomography. *Optics letters*, 2004, vol. 29, no. 14, pp. 1647-1649. ISSN 1539-4794.

[59] ZAGAYNOVA, E. et al. Contrasting properties of gold nanoparticles for optical coherence tomography: phantom, in vivo studies and Monte Carlo simulation. *Physics in Medicine and Biology*, 2008, vol. 53, no. 18, pp. 4995. ISSN 0031-9155.

[60] REGE, K. a MEDINTZ, I. L. *Methods in Bioengineering: Nanoscale Bioengineering and Nanomedicine*. Artech House, Incorporated, 2014. 365 pp. ISBN 9781596934115.

[61] JOSHI, M. et al. Characterization techniques for nanotechnology applications in textiles. *Indian Journal of Fibre and Textile Research*, 2008, vol. 33, no. 3, pp. 304-317.

[62] MATERIALS EVALUATION AND ENGINEERING, I. Scanning Electron Microscopy. 2014, [cit. 23.07. 2015]. Available from:<http://www.mee-inc.com/files/1014/2118/3300/HAMM_2014-ScanningElectronMicroscopy.pdf>.

[63] NANOSCIENCE INSTRUMENTS, I. Scanning Electron Microscopy. [online]. 23.07. [cit. 23.07. 2015]. Available from: <http://www.nanoscience.com/products/sem/>.

[64] PLASTICPHOTOVOLTAICS.ORG. UV-vis spectroscopy. [online]. 23.07. [cit. 23.07. 2015]. Available from: <http://plasticphotovoltaics.org/lc/characterization/lc-advanced-c/lc-uvvis.html>.

[65] NANOCOMPOSIX. UV/VIS/IR SPECTROSCOPY ANALYSIS OF NANOPARTICLES. 2012, [cit. 23.07. 2015]. Available from:<http://50.87.149.212/sites/default/files/nanoComposix%20Guidelines%20for%20UV-vis%20Analysis.pdf>.

[66] CHEN, Z. et al. UV-Vis Spectroscopy. In *Photoelectrochemical Water Splitting*. Springer New York, 2013, pp. 49-62.

[67] PONCE DE LEON, Y. et al. Contrast Enhancement of Optical Coherence Tomography Images Using Branched Gold Nanoparticles. *Journal of Nanomaterials*, 2012, vol. 2012, pp. 9.

[68] MATERIALS EVALUATION AND ENGINEERING, I. Fourier Transform-Infrared Spectroscopy (FTIR) [online]. 23.07. [cit. 23.07 2015]. Available from: <http://www.mee-inc.com/hamm/fourier-transform-infrared-spectroscopy-ftir/>.

[69] NICOLET, T. *Introduction to Fourier Transform Infrared Spectrometry* [online]. 2011 [cit. 21.07. 2015].

[70] EUROPE, W. T. How DLS works. [online]. 21.07. [cit. 21.07. 2015]. Available from: <http://www.wyatt.eu/index.php?id=how-dls-works>.

[71] LTD, M. I. Dynamic Light Scattering: An Introduction in 30 Minutes [online]. 21.07. [cit. 21.07. 2015]. Available from: <http://www.nanobiotec.iqm.unicamp.br/download/particles-Artigo%20Malvern.pdf>.

[72] INSTRUMENTS, L. Dynamic Light Scattering: Measuring the Particle Size Distribution. [online]. 21.07 [cit. 21.07. 2015]. Available from: <http://www.lsinstruments.ch/technology/dynamic_light_scattering_dls/>.

[73]   SIESLER, H. W. et al. *Near-Infrared Spectroscopy: Principles, Instruments, Applications*. Wiley, 2008. pp. ISBN 9783527612673.

[74]   A. SARKAR, M. L. Near Infra Red Spectroscopy: Redefining the ways to evaluate some of the critical parameters in hydrocarbon Industry 2010, [cit. 23.07. 2015]. Available   from:<http://www.petrotechsociety.org/wp-content/themes/continuum/pdf/20100757-FP.pdf>.

[75]   BLANCO, M. a VILLARROYA, I. NIR spectroscopy: a rapid-response analytical tool. *TrAC Trends in Analytical Chemistry*, 2002, vol. 21, no. 4, pp. 240-250. ISSN 0165-9936.

[76]   NANOCOMPOSIX. 980 nm Resonant Gold Nanoshells. [online]. 20.04. [cit. 28.07. 2015]. Available from: <http://nanocomposix.eu/collections/nanoshells/products/980-nm-resonant-gold-nanoshells>.

[77]   NANOPARTZ. Nanopartz Gold Nanorodz. [online]. 23.07. [cit. 23.07. 2015]. Available from: <http://www.nanopartz.com/bare_gold_nanorods.asp>.

[78]   NIKABADI, H. R. et al. Gradual growth of gold nanoseeds on silica for SiO2@ gold homogeneous nano core/shell applications by the chemical reduction method. *Physica Scripta*, 2013, vol. 87, no. 2, pp. 025802. ISSN 1402-4896.

[79]   THORLABS OCS1300SS Swept Source OCT System, User Guide 2011, pp. 27.

[80]   THORLABS. Callisto 930 nm OCT Imaging System. [online]. 10.04. [cit. 29.07. 2015].   Available   from: <http://www.thorlabs.de/newgrouppage9.cfm?objectgroup_id=3779>.

[81]   THORLABS Optical Coherence Tomography, ThorImage OCT, Operating Manual 2014, pp. 60.

[82]   HALAS, N. J. Gold Nanoshell Synthesis. [online]. 24.07 [cit. 24.07 2015]. Available from: <http://education.mrsec.wisc.edu/SlideShow/slides/nanoparticles/Au_nanoshell_synthesis.html>.

[83]   HADDADA, M. B. et al. Optimizing the immobilization of gold nanoparticles on functionalized silicon surfaces: amine-vs thiol-terminated silane. *Gold Bulletin*, 2013, vol. 46, no. 4, pp. 335-341. ISSN 2190-7579.

[84]   BRINSON, B. E. et al. Nanoshells made easy: improving Au layer growth on nanoparticle surfaces. *Langmuir*, 2008, vol. 24, no. 24, pp. 14166-14171. ISSN 0743-7463.

[85]   KARDYS, A. Y. et al. Amino-functionalized silica nanoparticles: in vitro evaluation for targeted delivery and therapy of pancreatic cancer. *Journal of Nanotechnology*, 2013, vol. 2013. ISSN 1687-9503.

[86]   NGHIEM, T. H. L. et al. Preparation and characterization of silica–gold core–shell nanoparticles. *Journal of nanoparticle research*, 2013, vol. 15, no. 11, pp. 1-9. ISSN 1388-0764.

[87]   YOUNG, J. K. et al. Size-controlled synthesis of monodispersed gold nanoparticles via carbon monoxide gas reduction. *Nanoscale research letters*, 2011, vol. 6, no. 1, pp. 1-11. ISSN 1931-7573.

[88]   LI, C. et al. Facile synthesis of concentrated gold nanoparticles with low size-distribution in water: temperature and pH controls. *Nanoscale research letters*, 2011, vol. 6, no. 1, pp. 1-10. ISSN 1931-7573.

[89]   IBRAHIM, I. A. et al. Preparation of spherical silica nanoparticles: Stober silica. *J. Am. Sci*, 2010, vol. 6, no. 11, pp. 985-989.

[90]   SUGIMOTO, T. *Fine Particles: Synthesis, Characterization, and Mechanisms of Growth*. Taylor & Francis, 2000. pp. ISBN 9780824700010.

[91]   ZIELECKA, M. Characteristics of silica nanopowders and sol containing immobilized nanoparticles of copper or silver. *Polimery*, 2011, vol. 56, no. 10, pp. 765-768. ISSN 0032-2725.

[92]   MILEA, C. et al. The influence of parameters in silica sol-gel process. *Bulletin of TheTransilvania University of Brasov*, 2011, vol. 4, pp. 53.

[93]   KANJANAWARUT, R. et al. UV-Vis Spectroscopy and Dynamic Light Scattering Study of Gold Nanorods Aggregation. *Nucleic acid therapeutics*, 2013, vol. 23, no. 4, pp. 273-280. ISSN 2159-3337.